

الجمهورية الجزائرية الديمقراطية الشعبية  
وزارة التعليم العالي والبحث العلمي  
PEOPLE'S DEMOCRATIC REPUBLIC OF ALGERIA  
MINISTRY OF HIGH EDUCATION AND SCIENTIFIC RESEARCH  
جامعة سعد دحلب البليدة 1  
UNIVERSITY OF SAAD DAHLEB BLIDA 1



كلية العلوم – دائرة الفيزياء  
Faculty of science  
Department of Physics

**Final Thesis**  
**For obtaining the Master's degree in Physics**

Option: Nanophysics

**Theme:**  
Finite Element Method Simulation and Performance Evaluation  
of  
MEMS Pressure Sensor Based on Capacitive Effect  
Using Comsol Multiphysics

**Presented by :**  
**SOUISSI MERIEM**

Defended on Sept. /29/2020 before the jury composed of:

Dr W. LASLOUNI	MCB	University of Blida 1	President
Dr A. HASSEIN-BEY	MCB	University of Blida 1	Examiner
Dr N. BELGROUNE	MCB	University of Blida 1	Supervisor

**BLIDA 2020**

**Abstract:**

In this final memoire of studies in Master of nanophysics, we discuss and describe the analysis and finite element methods (FEM) simulation of electro-mechanical effects of Micro-electromechanical systems (MEMS) based capacitive pressure sensor with high pressure sensitivity and small size. This model uses the Electro-mechanics interface (EMI) implemented in Comsol Multiphysics software.

This study focuses on the diaphragm deflection, sensitivity and capacitance versus pressure analysis and thermal considerations. Also the simulation results emphasize the importance of considering packaging in the MEMS design process. It also describes comparison of sensitivity of capacitive pressure sensor with and without packaging stress. Specific materials have been used (Molybdenum, Tungsten) in the simulation instead of material Silicon.

**Keywords:**

MEMS, Capacitive Sensors, Comsol Multiphysics, FEM.

**المخلص:**

في هذه المذكرة النهائية للدراسات في ماستر نانوفيزياء ، نناقش ونصف التحليل ومحاكاة طريقة العناصر المنتهية (FEM) للتأثيرات الكهروميكانيكية لمستشعر الضغط السعوي القائم على النظم الكهروميكانيكية الصغرى (MEMS) مع الحساسية العالية للضغط وصغر الحجم. يستخدم هذا النموذج واجهة الميكانيكا الكهربائية (EMI) المدمجة في برنامج Comsol Multiphysics. تركز هذه الدراسة على انحاء الحجاب الحاجز والحساسية والسعة بدلالة تحليل الضغط والاعتبارات الحرارية. كما تؤكد نتائج المحاكاة على أهمية مراعاة التغليف في عملية تصميم نظام MEMS. كما تصف مقارنة حساسية مستشعر الضغط السعوي مع أو بدون إجهاد التغليف. لقد استخدمت مواد محددة (الموليبدنوم ، التنجستن) في المحاكاة بدلاً من مادة السيليكون.

**Resumé:**

Dans ce mémoire final des études en Master de nano-physique, nous discutons et décrivons l'analyse et la simulation par la méthode des éléments finies (FEM) du comportement électromécanique du capteur de pression capacitif basé sur MEMS avec une sensibilité à haute pression et de petite taille. Ce modèle utilise l'interface électromécanique (EMI) implémentée dans le logiciel Comsol Multiphysics.

Cette étude se concentre sur la déflexion du diaphragme, la sensibilité et la capacité par rapport à l'analyse de la pression et aux considérations thermiques. Les résultats de la simulation soulignent également l'importance de la prise en compte de l'intégration dans le processus de conception des microsystèmes. Elle décrit également la comparaison de la sensibilité du capteur de pression capacitif avec ou sans contrainte d'intégration. Des matériaux spécifiques ont été utilisés (molybdène, tungstène) dans la simulation à la place du matériau silicium.

## **Dedication**

To My Parent.

To My Husband.

To Our children.

## **Acknowledgement**

First of all, I thank Allah to give me force, courage and good opportunity to do this work.

I would like to thank my thesis supervisor Dr. N. BELGROUNE of the Faculty of Sciences at the University of Blida, USDB-1. Thanks for him, to trust in the continuation of my work even with the pandemic situation, to guide me in the redaction and completion of this manuscript.

Also, my thanks are sent to all Teachers, I known during my life, starting with my first teacher, my Father, and finishing with Dr. A. HASSEIN-BEY, Dr. A. BENHAFFAF and all teachers of nanophysics graduated class I have had.

I would like to thank the experts who were involved in the validation survey for this research project: Dr. W. LASLOUNI as the President of the Jury and Dr. A. HASSEIN-BEY as the Examiner of this thesis. Without their input, the validation survey could not have been successfully conducted especially during these challenging times.

At last, I would like to thank my husband and my son who both comforted me along this way by their warm presence and sincere encouragements.

## List of figures:

Figure 1. 1: Micro mirror arrays [14].	P12
Figure 1.2: Cross-sectional schematic of a piezo-resistive pressure [15].	P14
Figure 1.3: Cross-sectional schematic of a capacitive pressure [15].	P15
Figure 1.4: Cross-sectional schematic of a touch-mode capacitive [15].	P16
Figure 1.5: Characteristic response of a touch-mode capacitive [15].	P17
Figure 1.6 : Poly-silicon surface micro-machined capacitive pressure sensors [19].	P18
Figure 1.7: Capacitance of a parallel plate capacitor.	P19
Figure 1.8: Capacitance of non parallel plate capacitor.	P20
Figure 2.1: A sample of triangular mesh for some structure generated by Comsol.	P23
Figure 2.2 : Conduction of heat in a rod of length L.	P25
Figure 2.3: Partition of the domain into a finite element grid.	P26
Figure 2.4: A primitive meshing.	P28
Figure 2.5: Linear approximation of the temperature over the element $e_i$ .	P28
Figure 2.6: Schematic of assembly process for the two elements system [59].	P30
Figure 2.7 : Shape functions in a general grid of piecewise linear elements. .	P31
Figure 2.8: Piecewise linear versus piecewise quadratic interpolation.	P31
Figure 2.9: A 2-D irregular mesh with triangular elements.	P33
Figure 2.10 : A typical 2-D linear triangular element.	P33
Figure 2.11 : Quadratic triangular element.	P34
Figure 2.12: Common 3-D elements: hexahedron; tetrahedron and cylindrical (Pentahedron).	P35
Figure 2.13: The silicon lattice unit cell [63].	P36
Figure 3.1: A 2D cross-section of capacitive pressure sensor.	P39
Figure 3.2: The device geometry model.	P40
Figure 3.3: Diagram flow of Modeling and Numerical Simulation Procedure.	P41
Figure 3.4 : Electromechanic Interface of Comsol Multiphysics.	P43

Figure 3.5: The Stationary study from the Preset Studies used for the modeling.	P43
Figure 3.6: The sensor geometry.	P44
Figure 3.7 : The lower face of the diaphragm subject of displacement.	P45
Figure 3.8.a: View of the YZ mirror plane.	P46
Figure 3.8.b : View of the XZ mirror plane.	P46
Figure 3.8.c: The Cavity of the sensor (Domain 3).	P46
Figure 3.9 : Definition of the no sliding reference point (44) of the sensor.	P47
Figure 3.10: The starting mesh boundary.	P49
Figure 3.11 : The extended mesh surface on the bottom of sensor.	P49
Figure 3.12 : The final generated mesh.	P50
Figure 4.1: $p_0(5)=20000$ Surface: Total displacement (mm).	P53
Figure 4.2: Maximum and mean displacement of the membrane vs the pressure and without packaging stresses.	P53
Figure 4.3: Diaphragm displacement (red curve) with packaging stresses. The green and blue curves are for unstressed device.	P54
Figure 4.4: Electric potential in the cavity of the capacitive sensor.	P55
Figure 4.5: Capacitance versus pressure, with and without the packaging stresses.	P55
Figure 4.6: Capacitance vs. Pressure for square diaphragm with packaging stress [63].	P56
Figure 4.7: The displacement (pressure of 20 kPa) with packaging stresses.	P57
Figure 4.8: Capacitance versus temperature.	P58

### List of tables

Table 3.1: Geometric specifications of the model.	P44
Table 3.2: Physical parameters imposed to the model.	P45
Table 4.1: The sensitivities of the studied capacitive pressure sensor.	P59
Table A.1: Layers thickness of the CPC.	P62
Table B.1: Physical proprieties of Silicon.	P67
Table B.2: Physical proprieties of Molybdenum.	P68
Table B.3: Physical proprieties of Tungsten.	P68

## Contents

	<b>Page</b>
Title .....	
Abstracts and keywords .....	
Dedication .....	
Acknowledgement .....	
List of figures .....	
List of tables .....	
<b>General introduction</b> .....	<b>09</b>
<b>Chapter 1: State of art of capacitive pressure sensors.</b> .....	<b>11</b>
1.1 Introduction .....	11
1.2 Some MEMS technology applications .....	11
1.3 Pressure Sensors .....	13
1.3.1 Piezo-resistive Sensors .....	14
1.3.2 Capacitive Sensors .....	15
1.4 Mathematics on Capacitive Pressure Sensor .....	18
1.5 Conclusion .....	20
<b>Chapter 2: Finite Element Method and Materials</b> .....	<b>21</b>
2.1 Introduction .....	21
2.2 Basic concepts of finite elements method .....	23
2.2.1 Method of Weighted Residuals and Galerkin Approximations .....	24
2.2.2 The weak statement Method .....	25
2.2.3 General treatment Method .....	30
2.3 Generalization of FEM to two and three dimensions .....	32
2.4 The meshing processes .....	32
2.5 An outline of some MEMS materials .....	35
2.5.1 Properties of Silicon .....	35
2.5.2 Properties of Molybdenum .....	37
2.5.3 Properties of Tungsten .....	37
2.6 Conclusion .....	38
<b>Chapter 3: Modeling and simulation</b> .....	<b>39</b>
3.1 Introduction .....	39

3.2 Design and Model concept of capacitive pressure sensor .....	39
3.3 Modeling instructions .....	41
3.3.1 Model Definition in Comsol Multiphysics .....	42
3.3.2 Geometry .....	43
3.3.3 GLOBAL DEFINITIONS .....	44
3.3.4 ELECTRO-MECHANICS INTERFACE (EMI) .....	46
a. Symmetry 1 .....	47
b. Symmetry 2.....	47
3.3.5 BOUNDARY CONDITIONS .....	47
a. Moving mesh boundary conditions .....	48
b. Prescribed Mesh Displacement 1.....	48
c. Terminal 1 and Ground 1.....	48
3.3.6 MATERIALS.....	48
3.3.7 THE MESH .....	49
3.4 The capacitive Sensor Studies .....	50
3.4.1 STUDY 1(without packaging stress) .....	50
3.4.2 STUDY 2(with packaging stress) .....	50
3.4.3 STUDY 3 (Effect of temperature with Constant pressure) .....	50
3.5 Conclusion .....	51
<b>Chapter 4: Results and Discussion .....</b>	<b>52</b>
4.1 Introduction .....	52
4.2 Diaphragm behavior analysis .....	53
4.2.1 Total displacement study without packaging .....	53
4.2.2 Total displacement study with packaging.....	54
4.2.3 Electrical potential study .....	54
4.3 Capacitance response discussion .....	55
4.3.1 Capacitance versus pressure .....	55
4.3.2 Capacitance versus operating temperature .....	57
4.4 Sensitivity analysis of capacitive pressure sensors .....	58
4.5 Conclusion .....	59
<b>General conclusion .....</b>	<b>60</b>
Appendix A: Geometry Instructions .....	62
Appendix B: Proprieties tables of MEMS materials .....	67
<b>References .....</b>	<b>69</b>



## GENERAL INTRODUCTION

The development of Microsystems for sensing, analyzing and actuating is necessary and demanded by the needs of the nowadays society. Only small and powerful systems have the capability to decrease consumption of resources. Microsystems combine and integrate miniaturized sensors, actuators and electronics in a single device. Progress in technology and science continue to move forward in making the fabrication and the conception of micro and nano-devices and systems possible for a variety of industrial, consumer, and biomedical applications. A range of Micro-Electro-Mechanical Systems (MEMS) devices have been produced, some of which are used for trading purpose [1-6].

One of the largest industrial applications of these devices is the MEMS pressure sensors. Integrated devices have been used in airbag deployment in automobiles since the nineties of the last century. These sensors for tire pressure measurements were designed for common usage in many modern applications of MEMS devices include : chemical sensors, gas sensors, space science, missile defense applications, Pico-satellites for space applications, hydraulic, pneumatic, and other consumer products.

The MEMS capacitive pressure sensors which are our main focus in this project, can work out many different sorts of detecting and measurement problems. These sensors can be unaltered by humidity, temperature, or mechanical distortion. They exhibit good screen effect against stray electric fields than inductive sensors which are not easily shielded against magnetic fields and gain more advantage over their piezoresistive pressure sensor counterparts due to high sensitivity, low power consumption, free from temperature effects, IC compatibility, etc...

In our modeling we will use the built-in finite element methods to model our capacitive pressure sensor. By going through the explanation of Finite Elements Methods (FEM), using the electromechanics interface by COMSOL Multiphysics software to resolve physical equations and gives an outline of some MEMS materials.

The work presented in this project is devoted to the study and simulation, using the finite element method (FEM) through the electromechanics interface by COMSOL Multiphysics software, of MEMS based capacitive pressure sensor with high pressure

sensitivity and small size,. This work includes diaphragm deflection, sensitivity and capacitance vs. pressure analysis and thermal considerations. The simulation results emphasize the importance of considering packaging in the MEMS design process. It also describes comparison of sensitivity capacitive pressure sensor with and without packaging stress. This thesis is structured as follows:

The first chapter is devoted to the state of the art of some MEMS devices and their application impact. We begin by locating our center of interest which revolves around the use of MEMS devices in measurement of the pressure using capacitive pressure sensors. Next, we present the knowledge necessary for modeling of this device.

In the second chapter, we present and give a brief description of the mathematical tool available, of Finite Elements Methods (FEM), implemented in different interface of Comsol Multiphysics software to resolve physical equations. We then list the main numerical procedure that gives approximate solutions to ordinary and partial differential equations and gives an outline of some MEMS materials.

The third chapter we will define the concept of the MEMS capacitive pressure sensor model used in this study. Subsequently, we present the operating principle of the model, the geometric description of this capacitive pressure sensor and the simulations of with square diaphragm using COMSOL Multiphysics, in order to be able to complete its design.

In the fourth chapter, we discuss the results of the simulation and especially we focus on the sensitivity of the sensor and its performance compared to other references. Several simulations with different materials are carried out but only results using Molybdenum are quoted. We also emphasize results of diaphragm deflection, sensitivity and capacitance vs. pressure analysis and thermal studies on capacitance due to packaging stress. Then, the results obtained at the micrometric scale will be analyzed. It also describes comparison of sensitivity of capacitive pressure sensor with and without packaging stress.

Finally, we end with the general conclusions drawn from our results and the perspectives of this work.

## **CHAPTER 1**

### **STATE OF ART OF CAPACITIVE PRESSURE SENSORS.**

#### 1.1 Introduction:

MEMS devices play key roles in many areas of progress. Fabricated sensors, actuators, and electronics are the most implemented components in a complete system for a special function. Microsystems combine and integrate miniaturized sensors, actuators and electronics in one device. That is why system integration is essential for a powerful device. Regarding reliability, performance, volume and cost, the system approach can improve the quality of a commercial product.

The pressure sensors for tire pressure measurements were designed for common usage in many modern applications of MEMS devices include: chemical sensors, gas sensors, space science, missile defense applications, Pico-satellites for space applications, hydraulic, pneumatic, and other consumer products.

This chapter reports the basic principles of some MEMS devices, their application impact. Due to our interest which concerns the use of MEMS devices in measurement of the pressure, we give the state of art of capacitive pressure sensors. Next, the necessary knowledge for the modeling of this device will be presented.

#### 1.2 Some MEMS technology applications

MEMS devices are used in magnetic storage systems (super-compact and ultrahigh recording-density magnetic disk drives) [7]. Many integrated head/suspension micro-devices have been fabricated for contact recording applications [8,9]. High band width, servo-controlled micro-actuators have been designed for track-density applications, which serve as the fine-position control element of a two-stage [10-13]. Small oscillated motors and actuators for tip-based recording schemes have been fabricated. A bunch of sensors are used in industrial, consumer, and biomedical applications. Various microstructures or micro-components are used in micro-instruments and other industrial applications, such as *micro-mirror* arrays which are based on microscopically small mirrors Figure 1.1.

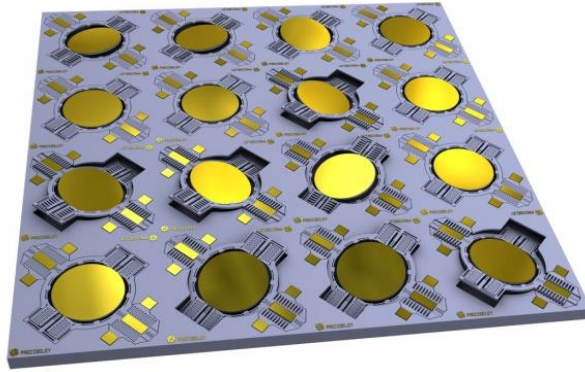


**Figure 1. 1:** Micro mirror arrays [14]

Bio-MEMS are used in commercial and defense applications. Applications of Bio-MEMS include

- Bio-fluidic chips for chemical and biochemical analyses and
- Biosensors in medical diagnostics to detect DNA, RNA, proteins, cells, blood pressure and toxin identification
- Biosensors in medical to deliver pharmaceutical drug.

Biosensors are designed to either detect a single or class of bio-chemicals or system-level analytical capabilities for a broad range of bio-chemical species known as micro Total Analysis Systems. The chips based on micro-fluidics involve the manipulation of tiny amounts of fluids in micro-channels using micro-valves for various analyses. The fluid is pumped into the chip using an external pump for analyses. Some chips have been designed with an integrated electro-statically actuated diaphragm-type micro pump. Silicon-based, disposable blood-pressure sensor chips were introduced in 90s by Nova-Sensor for blood pressure monitoring. After the of 9/11 events, concern over biological and chemical threat has led to the emergence of handheld units with bio- and chemical sensors for the detection of biological germs, chemical or nerve agents. It follows after 2001 a wide public usage of chemical precursors to protect population in subways, airports, and through the water supply. Other applications of BIOMEMS include endoscopic surgery, laser angioplasty (a medical procedure to widen arteries) and microscopic surgery. Implantable artificial organs of nano–size are also produced. Micro-instruments and micro-manipulators are used to do different actions on objects and features of nano-scale. Miniaturized analytical apparatus comprises gas chromatography and mass spectrometry. Other devices

include micro Scanning Tunneling Microscope (STM). Various examples of NEMS include [15]

- Nano version of components, devices, systems, and materials, such as micro-cantilever for STM and atomic force microscopy (AFM),
- AFM array (millipede) for data storage,
- AFM tips for nanolithography for printing molecules,
- Biological (DNA) motors,
- Molecular gears,
- Nanowires, carbon nanotubes,
- Quantum wires (QWRs), quantum boxes (QBs), and quantum transistors.

BIO-NEMS include nano biosensors which are microarray of silicon nano-wires, about a few nm in size. The biosensors act selectively to bind and to detect even a single biological molecule, such as DNA or protein. This is done by using nano-electronics to detect the slight electrical charge caused by such binding. Implantable drug-delivery devices or drug molecules are realized by automated shells for a specific target application, and silicon capsule with a nano-porous membrane filled with drugs for very slow delivery. Nano-devices for sequencing single molecules of DNA actually is use in the Human Genome Project. Cellular growth use carbon nano-tubes for spinal cord fixing.

Nano-electronics can be used to build: computer memory, using individual molecules or nano-tubes to store bits of information, molecular switches, molecular or nano-tube transistors, nanotube flat-panel displays, nanotube integrated circuits, fast logic gates, switches, nanoscopic lasers, and nanotubes as electrodes in fuel cells.

### 1.3 Pressure Sensors

Pressure sensors are among the first devices built by silicon micromachining technologies, having successful commercial benefit and widely used in industrial and biomedical applications. The sensors use piezoelectric, piezo-resistive, capacitive, and resonant sensing physical mechanisms. Silicon substrate and surface micromachining techniques have been used to make the details of sensors, thus reducing both their size and cost. Two families of pressure sensors exist: piezo-resistive family and capacitive family. They will be described below.

### 1.3.1 Piezo-resistive Sensors

The piezo-resistive phenomenon in silicon is well known physical effect and has been widely used in the pressure sensors fabrication process. A pressure induced strain deforms the silicon bulk and thus modifying the band structure states (gap and valence bands), leading to a change in the resistivity of the material. The piezo-resistivity is an anisotropic effect, meaning it is crystal-orientation dependent. It is also affected by the rate of doping and the degree of temperature. A conventional piezo-resistive pressure sensor can be implemented by manufacturing four sensing resistors along the edges of a thin silicon diaphragm.

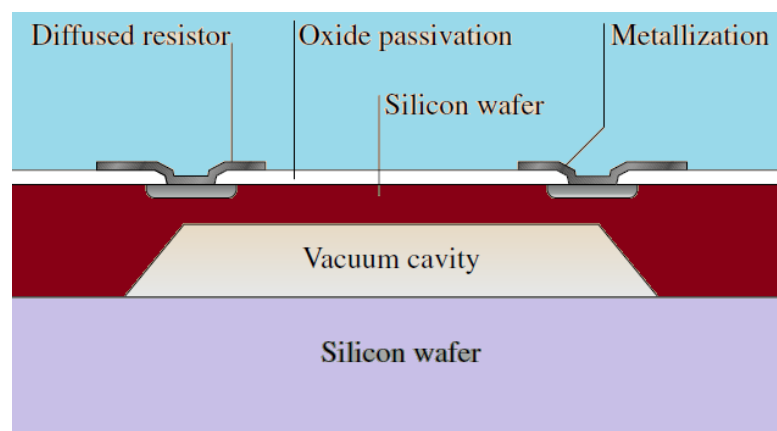


**Figure 1.2:** Cross-sectional schematic of a piezo-resistive pressure [15].

These system acts as a mechanical amplifier to amplify the stress and strain on the silicon target. The resistors elements are connected in a bridge configuration dotted with a push-pull signals to increase the sensitivity. For such a sensor and depending on the design, the measurable pressure ranges from  $10^{-3}$  to  $10^{+2}$  torr [15]. An example of a piezo-resistive pressure sensor is shown in Figure 1.2. The system consists of a silicon diaphragm hanging up over a reference vacuum cavity to figure an absolute pressure sensor. A certain external pressure value applied over the diaphragm induces a stress on the sensing resistors, leading to a resistance value change corresponding to the input pressure. The fabrication steps are as follows. The piezo-resistors are

- First fashioned through a boron diffusion process,
- Followed by a high temperature annealing (a cooking process). The objective of this step is to attain a resistance value on the order of a few kilo-ohms.
- The wafer is then covered with a silicon dioxide layer (insulator),
- The wafer is provided with opened windows for metallization.

- At this stage, the wafer is decorated on the backside, where a timed silicon wet etch to form the diaphragm is realized. The typical thickness of the diaphragm is around a few tens of micrometers and a length of several hundreds of micrometers.
- To complete the fabrication process, a second silicon wafer is then glued to the bottom device wafer in a vacuum to form a reference vacuum cavity.
- The bottom wafer can also be engraved through to form an inlet port.

Piezo-resistive sensors are easy to manufacture and can be incorporated with electronic systems. However, the resistors are temperature dependent and consume electric power. Further piezo-resistive sensors have proprieties which are not easy to characterize and are unstable in long terms. Further, they possess “resistor thermal noise”, thus limiting the sensors resolution.

### 1.3.2 Capacitive Sensors

Capacitive pressure sensors are very interesting because they are practically temperature independent and consume less power. The devices don't show initial turn-on adaptation time (functioning instantaneously) and are stable over time. In addition, Complementary Metal Oxide Semi-conductor (CMOS) microelectronic circuits are compatible when interfaced with capacitive sensors to provide advanced signal conditioning and processing, thus improving in general system performance. A sample of a capacitive pressure sensor is shown in Figure 1.3.

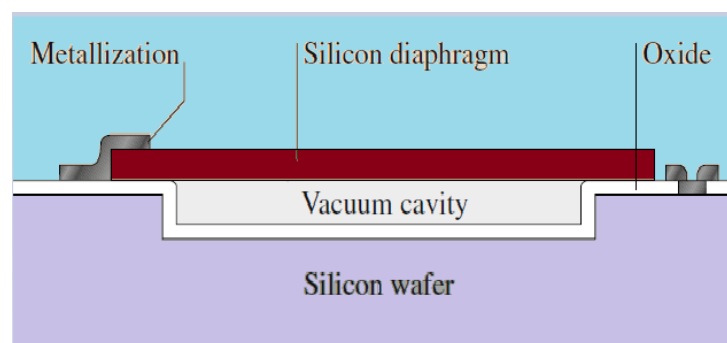


**Figure 1.3:** Cross-sectional schematic of a capacitive pressure [15].

The tool consists of a tight silicon diaphragm and hanging over a vacuum cavity. The diaphragm can be square or circular with few micrometers of thickness and a few hundred micrometers of size. The vacuum cavity has a depth of a few micrometers. The diaphragm and substrate form a variable capacitor which is pressure dependent. An augmentation in the external pressure deflects the diaphragm downward. As a result the capacitance value increases. A basic fabrication process can be outlined as follows:

- A silicon wafer is designed and etched to form the cavity.
- The wafer is oxidized and attached to a second silicon wafer with a heavily doped boron layer, which defines the diaphragm thickness.
- The bonding process is performed in a vacuum to realize the vacuum cavity.
- Alternatively a low-pressure sealing process can be used to form the vacuum cavity, provided that sealing channels are available.
- The silicon substrate above the boron layer is removed through a wet etching process,
- A patterning is performed to form the sensor diaphragm, playing the role of top electrode.
- Contact points are shaped by metallization.

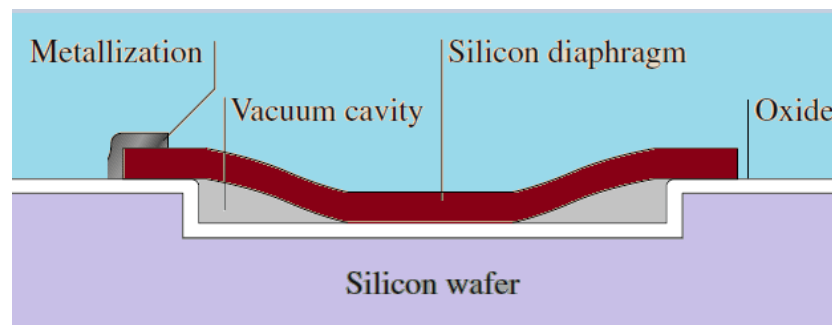


**Figure 1.4:** Cross-sectional schematic of a touch-mode capacitive [15].

The above pressure sensor shows a nonlinear behavior and a limited active range. These non desired effects can be attenuated by applying a modified architecture giving an electrostatic-force balanced feedback.

A ordinary practice, given in reference [16], is to introduce another electrode over the sensing diaphragm through wafer bonding, thus forming two capacitors in series. The capacitors are linked to electronic circuits which convert the sensor capacitance value to an output voltage corresponding to the diaphragm deformation. This signal voltage is analyzed to generate an electrostatic pull up force signal at the top electrode to maintain the deflectable diaphragm at its nominal position. This negative feedback action optimizes the nonlinearity behavior and extends the sensor dynamic range.

Another way to achieve a capacitive pressure sensor with intrinsic linear characteristic response and a large dynamic range is to employ the touch mode architecture [17]. The cross-sectional view of a touch-mode pressure sensor is illustrated in Figure 1.4. The device consists of an edge-clamped silicon membrane suspended over the vacuum



cavity. After deflecting under the external pressure, the diaphragm touches the bottom substrate. At this touch point more pressure will cause a linear increase in the sensor capacitance value. Figure 1.5 shows a typical device behavior curve with a turn point when the diaphragm reaches the bottom substrate. The touch point pressure can be adjusted by controlling the sensor geometric parameters (diaphragm size, thickness, cavity depth) according to the specific application requirements. The process flow to fabricate the device is similar to the basic capacitive pressure sensor. A typical fabricated touch-mode sensor employs a circular diaphragm with a diameter of  $800\ \mu\text{m}$  and a thickness of  $5\ \mu\text{m}$  suspended over a  $2.5\ \mu\text{m}$  vacuum cavity. The device achieves a touch point pressure of 8 psi ( $1\ \text{psi} = 6894,76\ \text{Pa}$ ) and the linear capacitance range starts from 33 pF at 10 psi up to 40 pF at 32 psi.

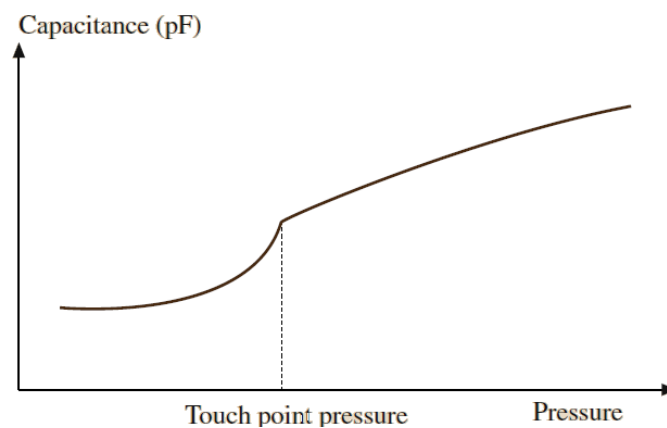


**Figure 1.5:** Characteristic response of a touch-mode capacitive [15].

All processes cited in the previous paragraphs use bulk silicon materials for machining. These processes are called bulk micromachining. The same devices can also be fabricated using surface micromachining. Surface micromachining technology is pretty for integrating MEMS sensors with on-chip electronic circuits. Consequently, highly developed signal processing capabilities can be implemented adjacent to micro-sensors on the same substrate. Those capabilities such as

- The data conversion,
- The offset and noise cancellation,
- The digital calibration,
- The temperature compensation,

provide a complete and high performance micro-system solution. The advantage of single chip is also to eliminate external wiring, which is very significant for minimizing background noise and enhancing system performance. Surface micromachining is a method

of depositing, patterning, and etching a sequence of thin films with thicknesses on the order of a micrometer in order to fabricate MEMS elements. A typical surface micromachining process flow starts by

- Depositing a layer of auxiliary material, such as silicon dioxide, over a wafer,
- Followed by anchor formation where a poly-silicon film is deposited and patterned.
- The underlying auxiliary layer is removed to liberate the suspended microstructure and finish the fabrication sequence.

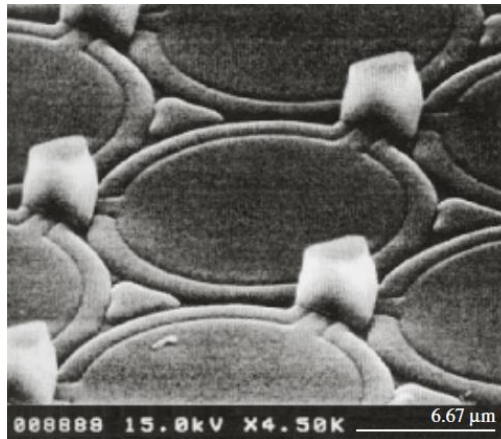


**Figure 1.6 :** Poly-silicon surface micro-machined capacitive pressure sensors [19].

The processing materials and steps are compatible with the standard integrated circuit process. They can be incorporated as an add-on module to an IC process [18]. As an example a surface micromachining technology has been performed to produce monolithic pressure sensor systems [19]. Figure 1.6 shows a Scanning Electron Microscope (SEM) micrograph of an array of MEMS capacitive pressure sensors fabricated on the same substrate. Each sensor has a circular poly-silicon membrane with  $0.8 \mu\text{m}$  of thick and a diameter on the order of  $20 \mu\text{m}$  closing a vacuum cavity of  $0.3 \mu\text{m}$  deep. The devices use the same operating principle as the sensor of Figure 1.3. These sensors have demonstrated efficiency in pressure ranges up to 400 bar with an precision of 1.5% [19].

#### 1.4 Mathematics on Capacitive Pressure Sensor

For a correct analysis of the fields and currents that make up a capacitive sensor, Maxwell's equations connecting electric and magnetic fields, charge density, and current density should be used. But a simplifying approximation which neglects magnetic fields and current is more or less possible with insignificant loss of accuracy. Systems in which this approximation is feasible are defined as electrostatic [20].

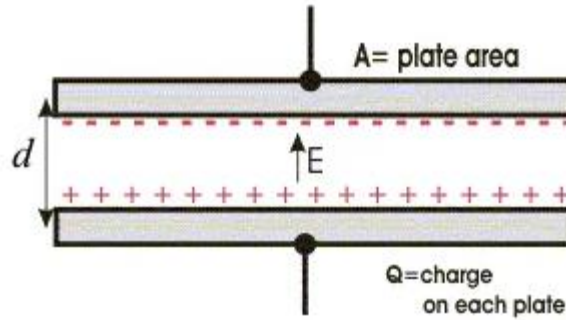


**Figure 1.7:** Capacitance of a parallel plate capacitor.

The problem of capacitor can be analyzed by application of Laplace's equation, a variant of one of Maxwell's equations. For the parallel plate geometry Figure 1.7, a voltage  $V$  can be applied to the plates to produce a total flux which, up a dielectric constant  $\epsilon_0$  depending on the unit system, is the electrical charge  $Q$ . Then, the amount of flux in coulombs which is produced by  $V$  volts is proportional to

$$Q = C V \quad (1.1)$$

The new symbol  $C$  is the capacitance of the plates in *coulombs/volt*. It is computed by the following expression

$$C = \frac{Q}{\int_0^d d\mathbf{l} \cdot \mathbf{E}} \quad (1.2)$$

The integral in the denominator is the circulation of the electrical field  $\vec{E}$  given by

$$\vec{E} = \frac{\sigma}{\epsilon_0} \vec{n}, \quad (1.3)$$

where  $\sigma = \frac{Q}{A}$  is the charge density of armature plate of area  $A$  and  $\vec{n}$  is an unit constant vector pointing to negative part of the capacitor. Putting altogether we obtain

$$C = \frac{\epsilon_0 A}{d} \quad (1.4)$$

If the space between is filled with some material of relative dielectric constant  $\epsilon_r$  the expression of  $C$  is

$$C = \frac{\epsilon_0 \epsilon_r A}{d} \quad (1.5)$$

In these expressions,  $d$  the distance separating the armatures is very small compared to capacitor shape. This approximation permits us to neglect the border effects on the electric field. In the case of a capacitor formed by two flat rectangular plates slightly inclined with respect to each other Figure 1.8, the distance  $d(x)$  will depends on the abscise  $x$ .

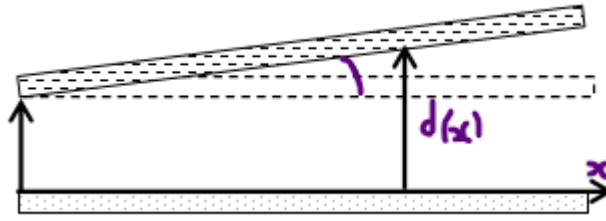


**Figure 1.8:** Capacitance of non parallel plate Capacitor

As a result the capacitance is computed as an integral of an infinitesimal element  $dC$  along the  $x$ -coordinate direction

$$C = \int dC = \int_0^a \frac{\epsilon_0 \epsilon_r dA}{d(x)} \quad (1.6)$$

For rectangular plate of large  $b$  and length  $a$ ,  $dA = b dx$  and  $x \in [0, a]$ , thus giving together with  $d(x) = d_0 + \tan(\alpha)x$  the expression of the total capacitance:

$$C = \frac{\epsilon_0 \epsilon_r b}{\tan(\alpha)} \ln \left( 1 + \frac{a \tan(\alpha)}{d_0} \right) \quad (1.7)$$

This expression shows the sensitivity to the inclination angle  $\alpha$  of the upper plate relatively to bottom plate.

In the current model of this thesis we deal with an upper plate played by diaphragm of the capacitive pressure sensor. The pressure effect on the diaphragm will generate a specific expression  $d(x)$  depending on the elasticity of the capacitor material. Any deformation yields to a change of the capacitance  $C$  of the device. These diaphragm deformations result from applied pressure or temperature change. From the above discussion we understand that a lot of care is taken in manufacturing pressure sensor to avoid residual deformation of the diaphragm by controlling geometry during bonding at temperature greater than room temperature.

### 1.5 Conclusion :

In this first chapter, we were able to introduce the state of the art in the field of MEMS technology. We first gave the basic principles of some MEMS devices and their application. Then, we presented the capacitive pressure sensors and the necessary knowledge for the modeling of these sensors.

Subsequently, we will treat the mathematical tool implemented in the interface of Comsol Multiphysics software to resolve physical equations, by going through the numerical procedure that gives approximate solutions to ordinary and partial differential equations. Thus, the following chapter will be devoted to the presentation and explanation of Finite Elements Methods (FEM).

## CHAPTER 2

### FINITE ELEMENT METHODS AND MATERIALS

#### 2.1 Introduction

The finite element method comes to existence since the middle of 1950s. The leading work on numerical solution of boundary valued problems traced back to the use of finite difference schemes; The starting of the finite element method emerged from these early mathematical methods and the difficulties associated with attempting to use FDM on less easy, geometrically irregular problems [21, 23].

In 50s, the efforts to solve continuum problems of elasticity medium began to appear using tiny and discrete elements to describe the overall behavior of simple elastic bars. Argyris [24] and Turner, et al. [25] were the first to apply their research for the aircraft industry. Clough is the first who coined the term "finite element" in his paper [26].

The finite elements techniques were first applied for structural-related problems. However, soon after others recognized the flexibility of the method and its underlying rich mathematical basis for application in non structural topics. Zienkiewicz and Cheung [27] were among the first to use the FEM to field problems as heat conduction, irrotational fluid flow, etc., by involving solution of Laplace and Poisson equations. Early work on non-linear problems can be found in Oden [28] and further discussions to model heat transfer problems with complex borders are found in Huebner work [29]; a complete 3-D finite element model for heat conduction is described by Heuser [30]. Application of the finite element technique to viscous fluid flow was initiated by Baker in 1971 [31].

Several articles have been published, and new applications appear regularly in the literature. Excellent reviews and descriptions of the method can be found in the earlier texts [32-40],. A strong mathematical discussion is given by Johnson [41], and programming the FEM is described by Smith [42]. A short monograph on development of the finite element method is given by Owen and Hinton [43].

The fundamental mathematical basis of the FEM lies with the classical Rayleigh-Ritz and variation computation procedures formulated by Rayleigh [44] and Ritz [45]. These linear theories explain why the FEM worked well for the class of problems with linear variation statements. However, as interest expanded in applying the FEM to more types of problems, as the case of fluid-related problems, the use of the above classical theory became limited and could not be applied.

Extension of the mathematical basis to non linear and non structural problems was realized through the method of biased residuals, originally achieved by Galerkin (1915). The method of biased or weighted residuals was conceived to provide the perfect theoretical set for a large basis of problems as opposed to the Rayleigh-Ritz method. Basically, the method needs the governing differential equation to be multiplied by a set of predetermined weights, followed by a global integration over space domain; the results of the integral are required to vanish. Galerkin's method is only a subclass of the general weighted residuals method, since various schemes of weights can be performed. In the case of Galerkin's method, the weights are chosen to be the same as the functions used to define the unknown variables.

The two Galerkin and Rayleigh-Ritz approximations yield matching results whenever a proper variational statement exists and the same basis functions are used. By using constant weights instead of functions, the weighted residual method yields the finite volume technique. A more deep description of the method of weighted residuals can be found in the work of Finlayson. Recent presentations of the method are discussed in Chandrupatla and Belegundu [46], Liu and Quek [47], Hollig [48], Bohn and Garboczi [49], Hutton [50], Solin et al [51], Reddy [52], Becker [53], and Ern and Guermond [54]. Actually, users of the FEM employ Galerkin's method to establish the approximations of the physical problem governing equations.

The introduction in the last decades of the finite element method through generalized mathematical solvers, such as MATHCAD [55], MAPLE [56], and MATLAB [57] and the supplementary software Comsol [58], have helped to spread the training and use of the method. The development of the FEM using these mathematical symbolic systems is described in numerous textbooks. Computer-based finite element analysis software packages that run on PCs can also be found on the web. In our modeling objective (chapter 4) we will use the built-in finite element methods of Comsol-Multiphysics to model our capacitive pressure sensor. Comsol is quite easy and very flexible – handling a wide range of problem classes including fluid flow (with turbulence), heat transfer,

structural analysis, electrodynamics, and general partial differential equations (PDE) including species transport, chemical reactions, and groundwater/porous media flows.

## 2.2 Basic concepts of finite elements method

The finite element method (FEM) is a numerical procedure that gives approximate solutions to ordinary and partial differential equations. It is aimed to model problems arising in physics and engineering. Like simple “finite difference schemes” (FDS) or “finite difference methods” (FDM) , the FEM requires a problem defined in geometrical space or domain, which is subdivided into a finite number of smaller regions, thus forming a mesh.

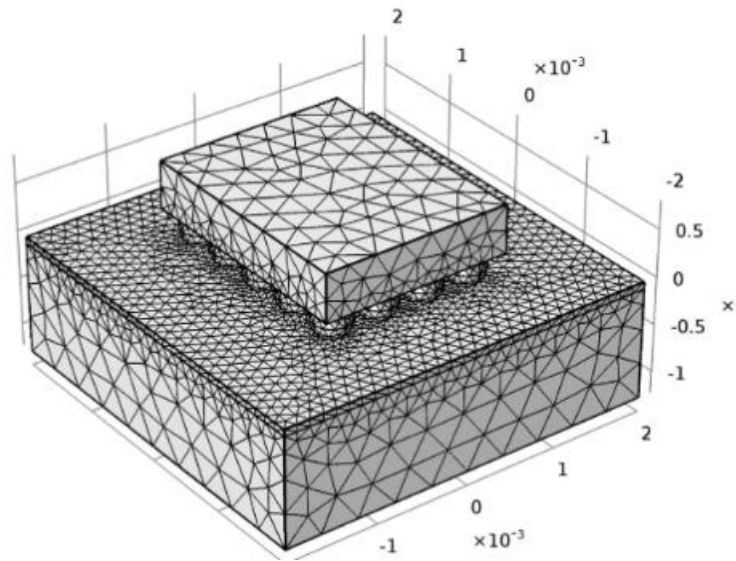


**Figure 2.1:** A sample of triangular mesh for some structure generated by Comsol.

In the above finite difference methods, the mesh is very simple consisting of rows and columns of orthogonal lines; however in finite elements methods, each subdivision is very particular for every problem and need not be orthogonal. For instance, triangles or quadrilaterals mesh can be used in two dimensions, and tetrahedral or hexahedral meshes in three dimensions Figure 2.1. Over each finite element of the domain, the unknown physical variables, as strain, temperature, velocity fields, etc., are approximated using known particular functions. The expressions of these functions can be linear or higher- order polynomial expansions in terms of the geometrical space variables around nodes used to define the finite element shape. In difference to finite difference procedures, the governing equations of the physical system in the finite element method are integrated over each finite element. The whole contributions are summed over the total problem space. As a consequence, finite linear equations are obtained in terms of the set of indefinite parameters

over the elements. Solutions of these equations are achieved using techniques of linear algebra.

The behavior of a event in a physical system, as static deformation or waves propagation, depends upon: the geometry or domain of the system, the property of the material or medium, the boundary, initial and loading conditions.

In computational modeling of physical system, the geometry or domain is in general very complex. Further, the boundary and initial conditions are also intricate. It is then, in general, very difficult to solve the governing differential equation analytically. Concretely, most of the problems are solved using numerical methods. The FEM are the most fashionable one, due to its practicality and flexibility. The process of computational modeling using the FEM mostly consists of 4 steps:

- Modeling of the geometry.
- Meshing (discretization).
- Specification of material property.
- Specification of boundary, initial and loading conditions.

When using the Finite Element Method to solve mechanics problems governed by partial differential equations, the concerned domain is first discretized into small elements. In all these elements, the outline of the shift or the displacement is assumed in simple forms to obtain element equations. These later are then putted together with adjacent elements to display the global finite element equation for the entire problem domain. Thus the obtained equations for the global problem domain can be solved easily for the displacement field. The FEM process described in above is not a difficult job. One can simply assume the profile of the solution of the displacements, but a principle has to guide us in order to obtain discretized system equations that can be solved normally for the final displacement field. This principle guarantees the nearest best solution of the governing system equation under certain conditions. In the next section we will introduce the basic concepts needed to develop approximations to the solution of differential equations that will ultimately lead to numerical algorithm of the finite element method. Through simple examples depicted from reference [59] we learn how the FEM works.

### 2.2.1 Method of Weighted Residuals and Galerkin Approximations

For this method, we follow two steps:

- First, let set up the weighted residuals form of the differential equations and give a general method leading to the weak formulation, which can be used to obtain finite element approximation of any kind of differential equation.



- Second, let introduce the concept of shape functions and the Galerkin approximation to the integral form of the governing differential equation.

As a toy model problem, we will consider heat conduction on a slender homogeneous metal wire of length  $L$  with a constant cross section. Assume that the left end is exposed to a prescribed heat flux,  $q$ , the right end is held at a constant temperature  $T_L$ , and the length of the rod is encircled by insulating material Figure 2.2.  $Q(x)$  is the magnitude of a volume heat source along the rod generated by electrical current.

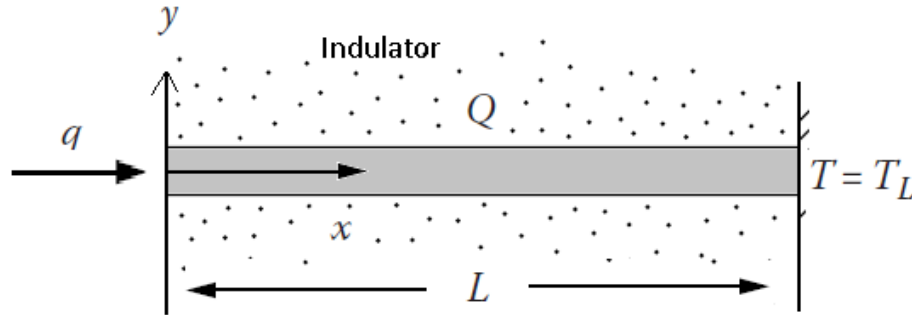


**Figure 2.2 :** Conduction of heat in a rod of length  $L$ .

The physical differential equation that controls the distribution of temperature  $T(x)$  across the rod is given by [59]:

$$-K \frac{d^2 T(x)}{dx^2} = Q(x), \quad x \in [0, L], \quad (2.1)$$

where  $K$  is the thermal conductivity constant of the material. The boundary conditions associated with the problem are

$$-K \left. \frac{dT(x)}{dx} \right|_{x=0} = q > 0, \quad T(x)|_{x=L} = T_L \quad (2.2)$$

The exact solution to differential equation with the above boundary conditions and assuming  $Q$  constant, is given by

$$T(x) = T_L + \frac{q}{K}(L - x) + \frac{Q}{2K}(L^2 - x^2) \quad (2.3)$$

This solution will be used to compare it with solutions obtained with the finite element procedure.

### 2.2.2 The weak statement method

The first step is to define a partition or grid in the interval  $0 < x < L$ , consisting of a finite number of non overlapping subintervals that wrap the full domain, as illustrated in Figure 2.3. Each subinterval  $e_k = \{x: x_k < x < x_{k+1}\}$  is called an *element*.

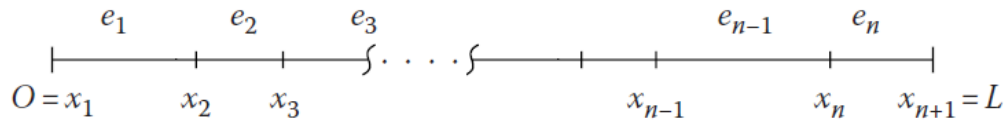


**Figure 2.3:** Partition of the domain into a finite element grid

The coordinates  $x_k$  are the ‘nodes’ abscises. Between two nodes  $x_j$  and  $x_{j+1}$ , the distribution of temperature is approximated using known, predetermined functions  $\Phi_j(x)$  (called shape functions), and corresponding unknown parameters  $a_j$ . For the whole rod  $0 < x < L$ , we can write

$$T(x) \cong a_1\Phi_1(x) + a_2\Phi_2(x) + \dots + a_{n+1}\Phi_{n+1}(x) \quad (2.4)$$

Or

$$T(x) = \sum_{j=1}^{n+1} a_j\Phi_j(x) \quad (2.5)$$

We will utilize the Galerkin form of the weighted residuals procedure to formulate the FEM method, that is to substitute the approximation (2.5) in the left-hand side of equation (2.1), but some “residual” difference  $R(T, x)$  will arise on the right-side, measuring how far we are from the exact solution  $T^*$ :

$$R(T, x) = -K \frac{d^2T(x)}{dx^2} - Q(x) \quad (2.6)$$

The idea of the weighted residuals method is that we can multiply the residual function  $R(T, x)$  by a weighting function  $W(x)$  and force the integral of the weighted expression to vanish:

$$\int_0^L W(x)R(T, x)dx = 0 \quad (2.7)$$

Or

$$\int_0^L W(x)K \frac{d^2T(x)}{dx^2} dx + \int_0^L W(x)Q(x)dx = 0 \quad (2.8)$$

Different choices of the weighting functions should be done to generate a system of linear equations in the unknown parameters  $a_j$ . The linear system is resolved using matrices algebra techniques. In the Galerkin procedure, the weights are set equal to the shape functions, that is,

$$W_j(x) = \Phi_j(x) \quad j = 1, 2, \dots, n + 1 \quad (2.9)$$

And we have

$$\int_0^L \Phi_j(x) K \frac{d^2 T(x)}{dx^2} dx + \int_0^L \Phi_j(x) Q(x) dx = 0 \quad (2.10)$$

The existence and uniqueness of the solution to the system of equations is assured if the boundary conditions associated with the differential equation are well posed. The question of how to define the shape functions  $\Phi_j(x)$  is where the technique of finite element methodology truly begins. The simplest choice is the linear, quadratic, and cubic interpolation polynomials but more choices, expensive in time and computational memory, are possible. We do not evoke mathematical details in the analysis of the problem. We just treat the case when the source is located in the position  $x_s$ :  $Q = \delta(x - x_s)$ , where  $\delta(x)$  is the Dirac function. The equation of heat propagation reads

$$-K \frac{d^2 T(x)}{dx^2} = \delta(x - x_s), \quad (2.11)$$

and has the following exact solution

$$T(x) = \begin{cases} -\frac{1}{K}(q(x-L) + (x_s - L)) + T_L & 0 \leq x \leq x_s \\ -\frac{1}{K}(1+q)(x-L) + T_L & x_s \leq x \leq L \end{cases} \quad (2.12)$$

In the Galerkin approach

$$\int_0^L \Phi_j(x) K \frac{d^2 T(x)}{dx^2} dx + \Phi_j(x_s) = 0 \quad (2.13)$$

After partial integration and assuming that  $K$  is a constant

$$\int_0^L K \frac{d\Phi_j(x)}{dx} \frac{dT(x)}{dx} dx - K \Phi_j(x) \frac{dT(x)}{dx} \Big|_{x=0}^{x=L} - \Phi_j(x_s) = 0 \quad (2.14)$$

This expression is called the weak form of (2.1). If the general case of a source and according to (2.10) we have

$$\sum_{j=1}^{n+1} K \left[ \int_0^L \frac{d\phi_i}{dx} \frac{d\phi_j}{dx} dx \right] a_j - \int_0^L \phi_i Q dx + \phi_i \left[ -K \frac{dT}{dx} \right] \Big|_{x=0}^{x=L} = 0 \quad (2.15)$$

$i = 1, 2, \dots, n+1$

Since the temperature is fixed at the end of the rod, the heat flux has to vanish there. This requires  $\Phi_{n+1}(L) = 0$ . It is the first condition required for shape functions. Let continue illustrating our example by splitting interval  $[0, L]$  into two equal length segments, with a node placed at both ends of each segment Figure 2.4.

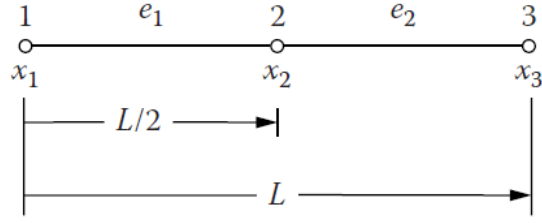


**Figure 2.4:** A primitive meshing.

If we assume that  $\Phi(x)$  between nodes are linear over each element  $e_i$ , then  $T(x)$  reads

$$T(x) = a_i \Phi_i(x) + a_{i+1} \Phi_{i+1}(x) \quad x_i \leq x \leq x_{i+1} \quad (2.16)$$

With the conditions  $\Phi_i(x_j) = \delta_{ij}$ , we can check that  $T(x_j) = a_j = T_j$  at the node  $j = 1, 2$  Figure 2.5. For the third node the temperature is known. Also the temperature  $T(x)$  is linear in the region  $x_i \leq x \leq x_{i+1}$  Figure 2.5.

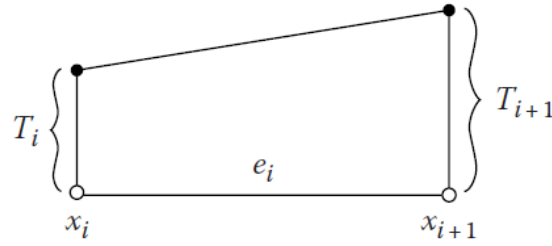


**Figure 2.5:** Linear approximation of the temperature over the element  $e_i$ .

A particular realization of the linear shape functions is as follow

$$\Phi_i(x) = \frac{x_{i+1} - x}{x_{i+1} - x_i} = 1 - \frac{2x}{L} \quad (2.17)$$

$$\Phi_{i+1}(x) = \frac{x - x_i}{x_{i+1} - x_i} = \frac{2x}{L} \quad (2.18)$$

Their derivatives are respectively

$$\frac{d\Phi_i(x)}{dx} = -\frac{1}{x_{i+1} - x_i} = -\frac{2}{L} \quad (2.19)$$

$$\frac{d\Phi_{i+1}(x)}{dx} = \frac{1}{x_{i+1} - x_i} = \frac{2}{L} \quad (2.20)$$

Let introduce the row vector and the column vector

$$\Phi = (\Phi_i \quad \Phi_{i+1}), \quad \mathbf{a} = \begin{pmatrix} a_i \\ a_{i+1} \end{pmatrix} \quad (2.21)$$

Their matrix product gives the temperature  $T(x)$ :

$$\Phi \cdot \mathbf{a} = (\Phi_i \quad \Phi_{i+1}) \cdot \begin{pmatrix} a_i \\ a_{i+1} \end{pmatrix} = T(x) \quad (2.22)$$

Then

$$\frac{d}{dx} \Phi \cdot \mathbf{a} = \left( \frac{d\Phi_i(x)}{dx} \quad \frac{d\Phi_{i+1}(x)}{dx} \right) \cdot \begin{pmatrix} a_i \\ a_{i+1} \end{pmatrix} = \frac{dT(x)}{dx} \quad (2.23)$$

The two equations of our system:

$$\begin{aligned} \sum_{j=1}^2 K \left[ \int_0^{L/2} \frac{d\phi_1}{dx} \frac{d\phi_j}{dx} dx \right] a_j - \int_0^{L/2} \phi_1(x) Q dx - K \phi_1(x) \frac{dT}{dx} \Big|_{x=0}^{x=L/2} &= 0 \\ \sum_{j=1}^2 K \left[ \int_0^{L/2} \frac{d\phi_2}{dx} \frac{d\phi_j}{dx} dx \right] a_j - \int_0^{L/2} \phi_2(x) Q dx - K \phi_2(x) \frac{dT}{dx} \Big|_{x=0}^{x=L/2} &= 0 \end{aligned} \quad (2.24)$$

become one matrix system

$$K \left[ \int_0^{L/2} \left[ \frac{d}{dx} \phi \right]^T \left[ \frac{d}{dx} \phi \right] dx \right] \mathbf{a} - Q \int_0^{L/2} \phi^T dx - \begin{bmatrix} q \\ 0 \end{bmatrix} = 0 \quad (2.25)$$

The upper index  $T$  stands for the transpose operation on a given vector. The flux  $q$  shows up because we treat only the first element  $e_1$  which contains the first node. The last system after integration leads to

$$\frac{2K}{L} \begin{bmatrix} 1 & -1 \\ -1 & 1 \end{bmatrix} \begin{bmatrix} a_1 \\ a_2 \end{bmatrix} - \frac{QL}{4} \begin{bmatrix} 1 \\ 1 \end{bmatrix} - \begin{bmatrix} q \\ 0 \end{bmatrix} = \begin{bmatrix} 0 \\ 0 \end{bmatrix} \quad (2.26)$$

For the second element  $e_2$  we will get a similar expression with null flux term:

$$\frac{2K}{L} \begin{bmatrix} 1 & -1 \\ -1 & 1 \end{bmatrix} \begin{bmatrix} a_2 \\ a_3 \end{bmatrix} - \frac{QL}{4} \begin{bmatrix} 1 \\ 1 \end{bmatrix} - \begin{bmatrix} 0 \\ 0 \end{bmatrix} = \begin{bmatrix} 0 \\ 0 \end{bmatrix} \quad (2.27)$$

The two last systems have four equations but we have three unknowns  $a_i$ . Re-assembling the second row of the first system with the first row of the second system we obtain the correct setting of the problem

$$\frac{2K}{L} \begin{bmatrix} 1 & -1 & 0 \\ -1 & 2 & -1 \\ 0 & -1 & 1 \end{bmatrix} \begin{bmatrix} a_1 \\ a_2 \\ a_3 \end{bmatrix} = \begin{bmatrix} q \\ 0 \\ 0 \end{bmatrix} + \frac{QL}{4} \begin{bmatrix} 1 \\ 2 \\ 1 \end{bmatrix} \quad (2.28)$$

In Figure 2.6 we have given a schematic of assembly process. The three temperature solutions follow from this matrix system and are

$$\begin{aligned}
 a_1 &= \frac{qL}{K} + \frac{QL^2}{2K} + T_L \\
 a_2 &= \frac{qL}{2K} + \frac{3QL^2}{8K} + T_L \\
 a_3 &= T_L
 \end{aligned}
 \tag{2.29}$$

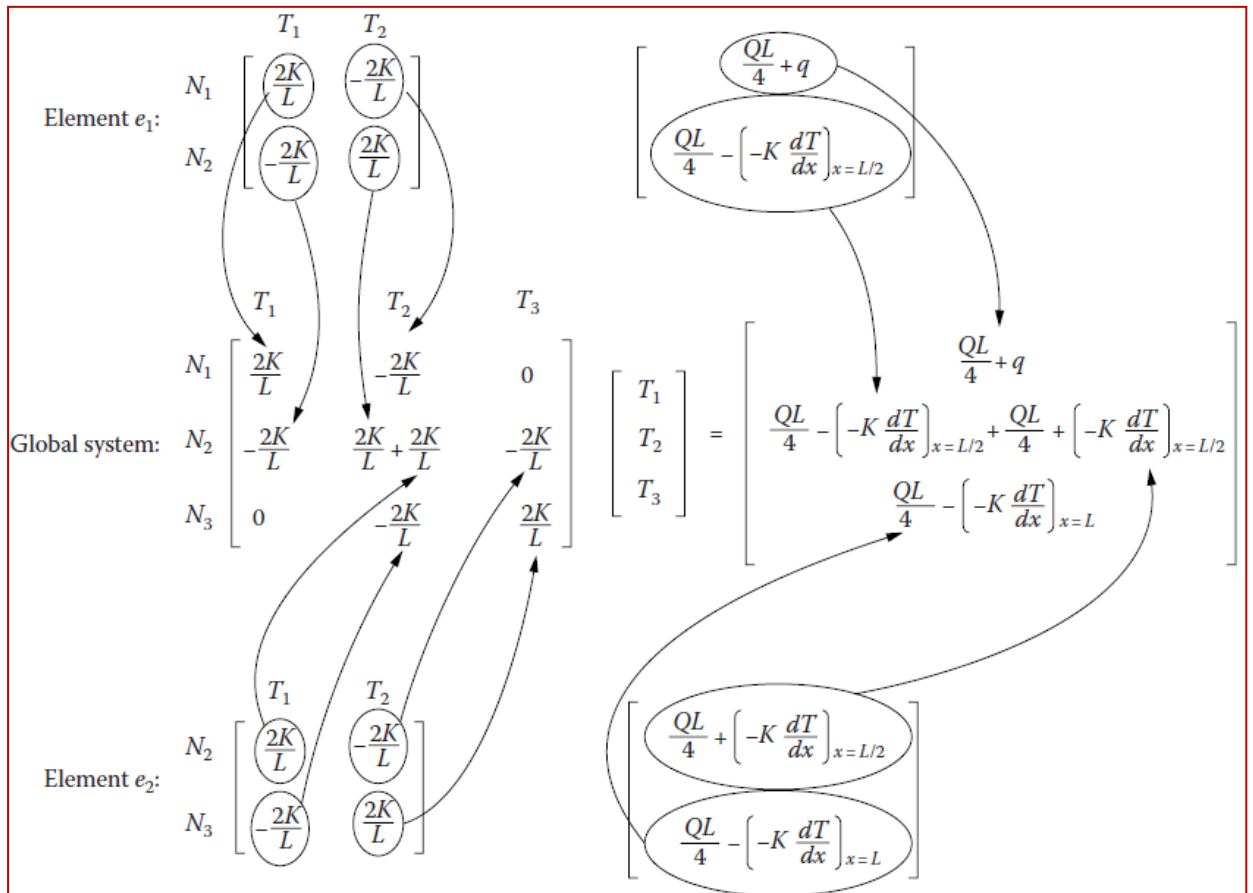


**Figure 2.6:** Schematic of assembly process for the two elements system [59].

### 2.2.3 General treatment Method:

If we want to upgrade to more precision on  $T(x)$ , we have to develop more details in the above example of heat propagation. For instance we can try to:

- arise the number of elements  $e_i$  in the region of study. This is called mesh refinement. The shape functions  $N_i(x)$  over elements  $e_i$  are piecewise linear elements with the propriety  $N_i(x_j) = \delta_{ij}$  ( $\delta_{ij}$  is the Kronicker symbol) Figure 2.7. The length of every element  $e_i$  is  $h_{(i)} = x_{i+1} - x_i$

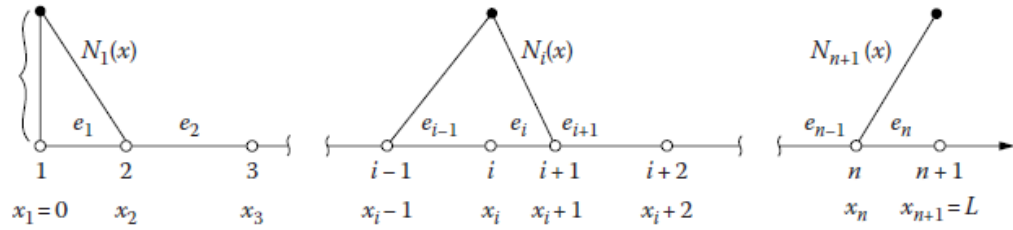


**Figure 2.7 :** Shape functions in a general grid of piecewise linear elements

- pass from linear shape functions to higher non linear functions (quadratic, cubic, etc.). This is called non linear interpolation between nodes. As example we can propose quadratic form of  $T(x)$  over element  $e$  Figure 2.8:

$$T^{(e)}(x) = \alpha_1 + \alpha_2 x + \alpha_3 x^2 \quad (2.30)$$

where  $\{\alpha_i\}$  are three coefficients determined by knowing the temperature over the two nodes of element  $e$  and a third added node in the middle. With this new node the length of the element  $e_i$  is  $h_i = x_{2i+1} - x_{2i-1}$ .

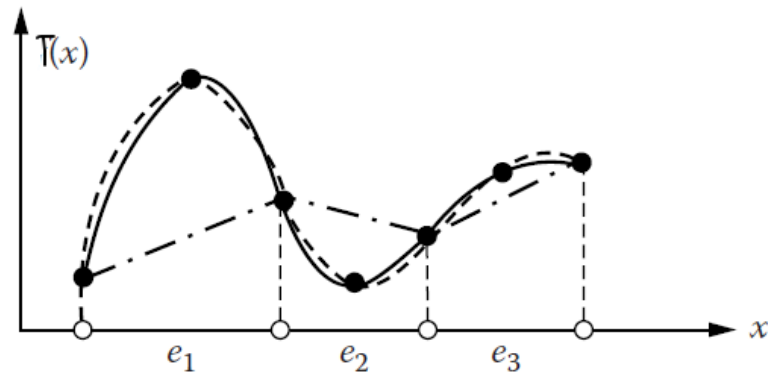


**Figure 2.8:** Piecewise linear versus piecewise quadratic interpolation

In this thesis we don't give technical details; we only quote the final results of the associated shape functions to the expression of the temperature over element  $e$ :

$$N_1^{(e)}(x) = 1 - 3 \frac{x}{h^{(e)}} + 2 \left[ \frac{x}{h^{(e)}} \right]^2 \quad (2.31)$$

$$N_2^{(e)}(x) = 4 \frac{x}{h^{(e)}} \left[ 1 - \frac{x}{h^{(e)}} \right] \quad N_3^{(e)}(x) = \frac{x}{h^{(e)}} \left[ 2 \frac{x}{h^{(e)}} - 1 \right]$$

And

$$T^{(e)}(x) = N_1^{(e)} T_1^{(e)} + N_2^{(e)}(x) T_2^{(e)} + N_3^{(e)}(x) T_3^{(e)} \quad (2.32)$$

We can proceed to even higher orders of approximation using steps. For cubic elements adding two nodes in every element  $e$  will give  $h_i = x_{2i+3} - x_{2i-1}$  and the shape functions of degree three.

Let notice that in FEM a natural coordinate system  $\xi$  is introduced for specifying the local operations on an element instead of a global coordinate  $x$ . This is done in the case of linear approximation through the transformation

$$x = \frac{1}{2}(1-\xi)x_i + \frac{1}{2}(1+\xi)x_{i+1} \quad (2.33)$$

and if quadratic approximation is used,

$$x = N_1(\xi)x_{2i-1} + N_2(\xi)x_{2i} + N_3(\xi)x_{2i+1} \quad (2.34)$$

Where

$$N_1(\xi) = \frac{1}{2}\xi(\xi-1) \quad N_2(\xi) = 1-\xi^2 \quad N_3(\xi) = \frac{1}{2}\xi(\xi+1) \quad (2.35)$$

### 2.3 Generalization of FEM to two and three dimensions

In the application problems, one discovers that most questions are not flexible to solution using one-dimensional analysis. On the other side, many problems can be studied and realistic solutions obtained using 2-D concepts. It is in the 2 and 3 dimensions problem domains that the strength of the FEM becomes evident. The concept of a mesh and the choices available for element discretization becomes significantly more important than in the 1-D examples discussed in above.

In 2-D problems, the physical domain is subdivided into sub-regions, or *elements*. Many polygonal forms can be used to define the *elements*. For example, rectangles are generally used when the problem domain itself is rectangular. However, rectangles don't easily fit well when the domain is irregular. The simplest geometric structure that easily accommodates irregular surfaces is the triangle, and it is one of the most element shapes ever used. Two additional constraints emerge when dealing with 2-D problems. The first constraint is that considerably more nodes will become involved in the solution process, thus leading to very large matrix inversion problem and a huge time for computer computation. Second, local mesh refinement is generally required in those regions where the variables of interest vary rapidly or where discontinuities exist. Today, many available finite element codes for structural analysis use a mixture of triangles and quadrilaterals for their mesh refinement.

### 2.4 The meshing processes

The element of the mesh is a triangle consisting of three vertex nodes Figure 2.9. In general, one sets more elements in those parts of the physical domain where functions are



expected to change more rapidly. When creating a triangular elements mesh, it is advised that elements be more closely placed in the direction of the largest *gradient*.

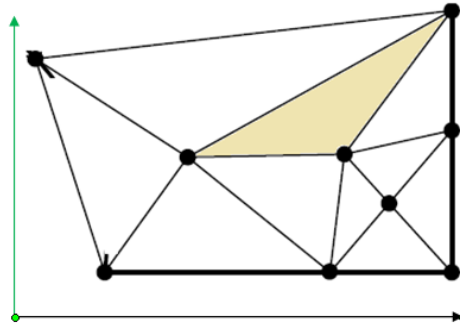


**Figure 2.9:** A 2-D irregular mesh with triangular elements

For the approximation of the field and shape functions we may use linear, three-noded elements (straight sides) which require many elements in order to reduce the error in the solution, or quadratic, curve-sided triangular elements which increases the accuracy. Examples meshes generated by Comsol are created using a mesh generator module that is included with Comsol 5.2 and in later version. To be close with the procedure commonly practiced in most FEM schemes, the local node numbers associated with a triangular element will be designated 1, 2, and 3 in a counterclockwise order Figure 2.10. The 2-D triangular element is represented by the polynomial of the form

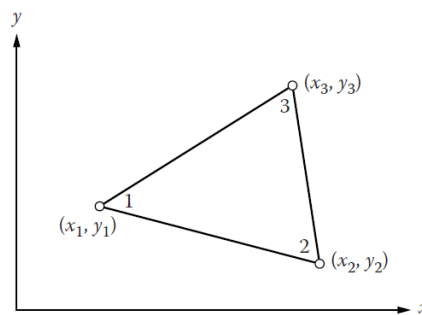


**Figure 2.10 :** A typical 2-D linear triangular element.

$$\phi = \alpha_1 + \alpha_2 x + \alpha_3 y \quad (2.36)$$

with three unknown coefficients. They are determined over the three nodes leading (after some algebra see Section 4.3.1 [59]) to the three shape functions

$$\begin{aligned} N_1^{(e)}(x, y) &= \frac{1}{2A^{(e)}} \left[ (x_2 y_3 - x_3 y_2) + (y_2 - y_3)x + (x_3 - x_2)y \right] \\ N_2^{(e)}(x, y) &= \frac{1}{2A^{(e)}} \left[ (x_3 y_1 - x_1 y_3) + (y_3 - y_1)x + (x_1 - x_3)y \right] \\ N_3^{(e)}(x, y) &= \frac{1}{2A^{(e)}} \left[ (x_1 y_2 - x_2 y_1) + (y_1 - y_2)x + (x_2 - x_1)y \right] \end{aligned} \quad (2.37)$$

where the area element  $A^{(e)}$  is introduced by

$$2A^{(e)} = (x_1y_2 - x_2y_1) + (x_3y_1 - x_1y_3) + (x_2y_3 - x_3y_2) \quad (2.38)$$

When a triangular quadratic element is used the interpolating polynomial is

$$\phi = \alpha_1 + \alpha_2x + \alpha_3y + \alpha_4x^2 + \alpha_5xy + \alpha_6y^2 \quad (2.39)$$

With six  $\alpha_i$ 's we have to three nodes, labeled (4,5,6), to the triangle Figure 2.11.

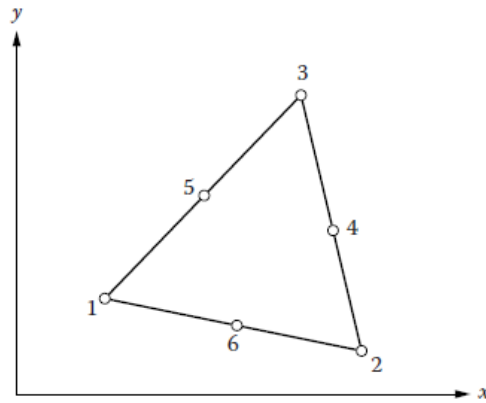


**Figure 2.11** : Quadratic triangular element

After this step 6 shape functions are computed consuming more effort and time. And this work is repeated for all triangles in the 2-D mesh. Some simplification are used by introducing the three area coordinates  $L_i$  fulfilling the proprieties

$$\begin{aligned} x &= L_1x_1 + L_2x_2 + L_3x_3 \\ y &= L_1y_1 + L_2y_2 + L_3y_3 \\ 1 &= L_1 + L_2 + L_3 \end{aligned} \quad (2.40)$$

These coordinates are equivalent to local coordinate  $\xi_i$  introduced in 1-D elements. The shape functions are expressed as function of  $L_i$  more easily in any approximation (linear, quadratic, etc.). Once one obtains the desired approximation of the field as a function of the shape functions he or she can uses weak statement process of Galerkin and achieves double integration  $\iint dx dy$  in  $(x, y)$  plane or equivalently the *constrained triple integration*

$$\iiint_{L_1+L_2+L_3=1} J dL_1 dL_2 dL_3. \quad (2.41)$$

After he or she has to solve linear system of unknown values of the field (temperature  $T(x, y)$  for example) over all the nodes of the mesh structure.  $J$  is a kind a Jacobian associated with the transformation from  $(x, y)$  plane to a 2-D surface embedded in the  $(L_1, L_2, L_3)$  space.

Extension of the finite element method to 3 dimensions follows from 2 dimensions theory. The quantity of data required to found the computational domain and boundary conditions turn out to be considerably greater over 2-D problems. Similarly, the amount of computational job increases significantly. Because of the additional number of nodes associated with the 3-D element the computational mesh is generally restricted. The tetrahedron and hexahedron elements are the fundamental bricks of mesh generation Figure 2.13. What we have given in this modest work is an evasive sight of Finite Element Methods and don't cover all the technical aspects which someone has to master in the purpose to conduct very suited computations for resolving physical equations such involved in the modeling of our capacitive pressure sensor.

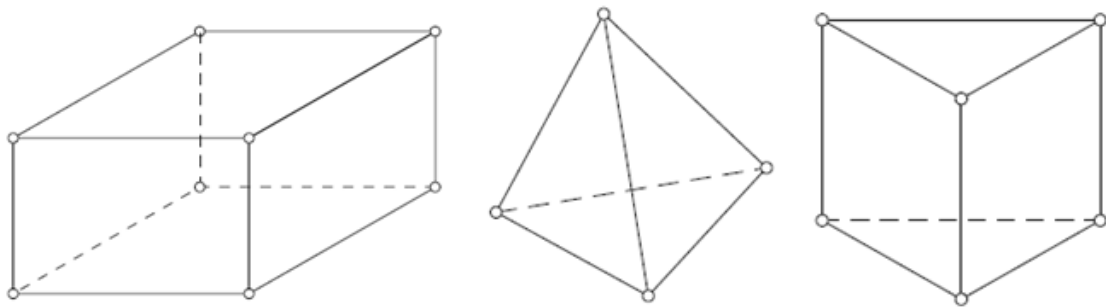


**Figure 2.12:** Common 3-D elements: hexahedron; tetrahedron and cylindrical (pentahedron).

## 2.5 An outline of some MEMS materials

### 2.5.1 Properties of Silicon

Silicon is an abundant atomic element existing in the Earth's layer (making up 25.7% of the Earth's crust) in different compounds. Silicon is present in the sun and stars and is a principal component of a class of meteorites known as "aerolites". It is also a component of tektites, a natural glass of uncertain origin. Natural silicon contains three isotopes. Twenty-four other radioactive isotopes are recognized. Silicon occurs as the oxide and as silicates, Sand, quartz, rock crystal, agate, flint and opal. Granite, hornblende, asbestos, feldspar, clay mica, etc. are but a few of the numerous silicate minerals. The principal proprieties are summarized table given in Appendix B.

Scientists in 1800 thought silica to be a compound and not an element; later in 1811, G. Lussac and co. prepared impure amorphous silicon by heating potassium with silicon tetrafluoride. Berzelius in 1824 succeeded in preparing amorphous silicon by the same general method as used earlier, but in addition he removes the fluosilicates by repeated washings. Deville in 1854 prepared crystalline silicon, the second allotropic form of the element.

Silicon is prepared by heating silica and carbon in an electric furnace, using carbon electrodes. Several other methods can be used for preparing the element. Amorphous silicon is prepared as a brown powder, which can be easily melted or vaporized.

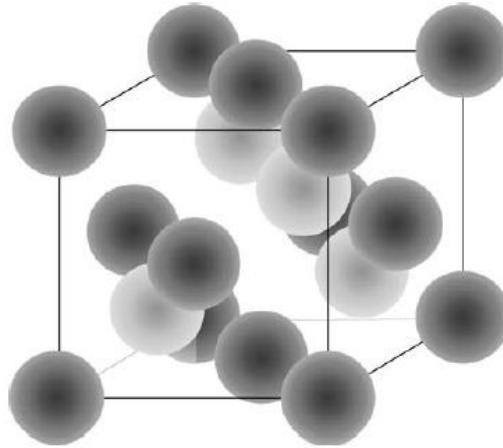


**Figure 2.13:** The silicon lattice unit cell. [63]

Crystalline silicon has a metallic shine and dull color. The Czochralski process is used to produce single crystals of silicon used for solid-state or semiconductor devices. Hyper-pure silicon is prepared by the thermal decomposition of ultra pure trichlorosilane ( $\text{SiHCl}_3$ ) in a hydrogen atmosphere, and by a vacuum float zone process. This product can be doped with boron, gallium, phosphorus, or arsenic to produce silicon for use in transistors, solar cells and other solid-state in electronics and space age industries.

Hydrogenated amorphous silicon has shown promise in producing economical cells for converting solar energy into electricity. Silicon is a relatively inert element, but it is attacked by halogens and dilute alkali. Silicones are important products of silicon. They may be prepared by hydrolyzing a silicon organic chloride. Hydrolysis and condensation of various substituted chlorosilanes are used to produce a great number of polymeric products, ranging from liquids to hard, glasslike solids with many useful properties. Silicon transmits more than 95% of all wavelengths of infrared, from 1.3 to 6.7  $\mu\text{m}$ . Silicon tetrachloride can be used to iridize glass. Silicon is a significant ingredient in steel; silicon carbide is one of the most important abrasives and has been used in lasers to produce coherent light of 4560  $\text{\AA}$ . Aerogel which is now used by NASA is a highly isolative material that has the lowest density of any known solid (~99.9% air and 0.1%  $\text{SiO}_2$  by volume). It is 1000 times less dense than glass and it is expected to trap cometary particles traveling at speeds of 32 km/sec. It has high thermal insulating qualities that could be used in home insulation. Its light weight may have aircraft applications.

### 2.5.2 Properties of Molybdenum

At first molybdenite was confused with graphite and lead ore. After, in 1778, Scheele recognized it as a distinct ore of a new element. The metal was obtained in an impure form in 1782 by Hjelm. Molybdenum does not occur in nature as simple element, but it is obtained mainly from molybdenite ( $\text{MoS}_2$ ). Wulfenite ( $\text{PbMoO}_4$ ) and powellite ( $\text{Ca}(\text{MoW})\text{O}_4$ ) are also minor commercial ores. Molybdenum is also derived as a by-product of copper and tungsten mining operations. The metal is produced from the powder made by the hydrogen reduction of purified molybdic trioxide or ammonium molybdate. Its thermal and mechanical properties are given in Appendix B. It has a silvery white color. It is very hard, but is softer and more ductile than tungsten. It has a high elastic modulus just after tungsten and tantalum. It is a valuable alloying agent, as it contributes to the hardenability and toughness of quenched and tempered steels. It also improves the strength of steel at high temperatures. It is used in certain nickel-based alloys, such as the Hastelloys which are heat-resistant and corrosion-resistant to chemical solutions. Molybdenum oxidizes at elevated temperatures. The metal has found recent application as electrodes for electrically heated glass furnaces. It is also used in nuclear energy applications and for missile and aircraft parts. Molybdenum is valuable as a catalyst in the refining of petroleum. It has found application as a filament material in electronic and electrical applications.

Molybdenum is an essential trace element in plant nutrition. Some lands are barren for lack of this element in the soil. Molybdenum sulfide is useful as a lubricant, especially at high temperatures where oils would decompose. Almost all ultra-high strength steels with minimum yield points up to 300,000 lb/in.<sup>2</sup> contain molybdenum in amounts from 0.25 to 8%. Natural molybdenum contains seven isotopes. Thirty other isotopes and isomers are known, all of which are radioactive.

### 2.5.3 Properties of Tungsten

Tungsten, or Wolfram, is a chemical element with the symbol W and atomic number 74. Tungsten is a rare metal found naturally on Earth combined with other elements in chemical compounds rather than alone. It was identified as a new element in 1781 and first isolated as a metal in 1783.

The free element is amazing for its strength. It has the highest melting point of all the elements discovered, see above table. It also has the highest boiling point, at 5930 °C (6200 K). Its density is 19.25 times that of water, comparable with that of uranium and gold, and much higher (about 1.7 times) than that of lead. Polycrystalline tungsten is a

basically brittle and hard material, making it difficult to work. Their thermal and mechanical properties are given in Appendix B. However, pure single-crystalline tungsten is more ductile and can be cut with a hard-steel hack saw.

Tungsten's many alloys have numerous applications, including incandescent light bulb filaments, X-ray tubes (as both the filament and target), electrodes in gas tungsten arc welding, Super alloys, and radiation shielding. Tungsten's hardness and high density give it military applications in penetrating projectiles. Tungsten compounds are also often used as industrial catalysts. Tungsten is known to occur in biomolecules, being found in a few species of bacteria and archaea. It is the heaviest element known to be essential to any living organism.

## 2.6 Conclusion

In computational modeling of physical system, the geometry or domain are in general very complex. Further, the boundary and initial conditions are also intricate. It is then, in general, very difficult to solve the governing differential equation analytically. Concretely, most of the problems are solved using numerical methods. The FEM are the most fashionable one, due to its practicality and flexibility.

In this second chapter, we presented the Finite Elements Methods (FEM). We have indeed given a brief description and properties of some MEMS materials available to use in our model of capacitive pressure sensors. Thus the chapter which follows will be devoted to the definition of the concept of MEMS Pressure Sensor Based on Capacitive Effect.

## CHAPTER 3 : MODELING AND SIMULATION

### 3.1 Introduction

This chapter describes the main object of our thesis, namely the simulation and performance analysis of capacitive pressure sensor with square diaphragm. We define the concept of the MEMS capacitive pressure sensor model used in this study. Subsequently, we present the operating principle of the model, the geometric description of this capacitive pressure sensor and the simulations of this square diaphragm using COMSOL Multiphysics software, in order to be able to complete its design. We will model diaphragm displacement, capacitance, sensitivity, linearity at different applied pressure of the sensors. Starting from existing studies [62-63], we follow the same instructions and goals to achieve our modeling and simulation. The difference resides in the type of materials we used.

### 3.2 Design and Model concept of capacitive pressure sensor

In chapter one, we have already introduced some prototype capacitive pressure sensors. We exhibit a structural design of capacitive pressure sensor. The proposed structure consists of two parallel plates acting as electrodes of capacitors and separated by air gap, thus forming a square die bonded to a wafer. Various parameters like type of material, size, shape and structure play a significant role in order to obtain optimized device with desired specification.

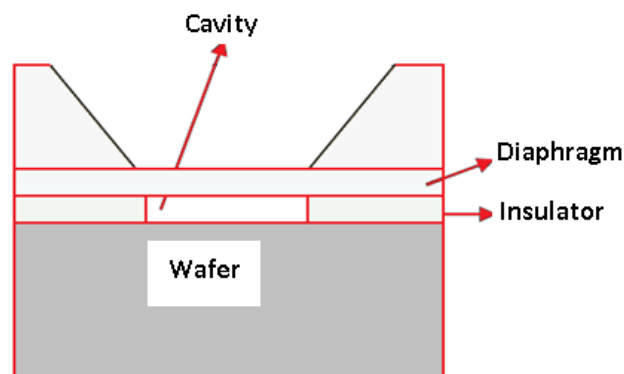


**Figure 3.1:** A 2D cross-section of capacitive pressure sensor.

A 2D section through the working part of the device is shown in Figure 3.1. The thin diaphragm is elevated to a fixed potential of 1 Volt. The membrane is separated from a ground plane cavity sealed under high vacuum. The lateral sides of the cavity are insulating to prevent an electrical connection between the diaphragm and the ground plane.

When the pressure over the sealed cavity changes the pressure difference causes the membrane to deflect. The thickness of the vacuum gap varies across the membrane and its capacitance to ground therefore changes. Thermal stresses are integrated into the structure as a result of the thermal conductivity difference between the material die and the material plate, especially when an elevated temperature is previously used for the industrial bonding process. These stresses change can alter the reading response of the sensor. Additionally, since the stresses are temperature function, the stresses introduce undesired effect to the device output.

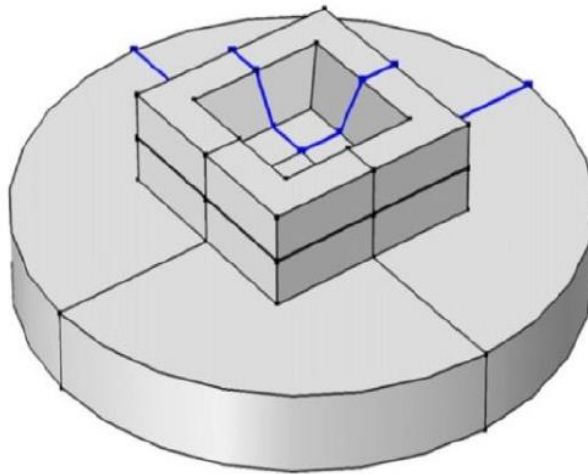


**Figure 3.2:** The device geometry model.

The full model geometry used as a capacitive pressure sensor is depicted in Figure. 3.2. It includes four quarters work symmetrically according to the two vertical mirror planes ( $x, z$ ) and ( $y, z$ ). Due to this symmetric geometry, only a single quadrant is modeled in COMSOL Multiphysics with symmetry boundary condition. This alternative will save memory and time of simulation.

The first main concerned material is a single crystal Molybdenum, having Young's Modulus of 312 GPa, Poisson's ratio of 0.31, density of  $10200 \text{ kg/m}^3$  (Data from Comsol Library). The dimension of square diaphragm is  $500 \mu\text{m} \times 500 \mu\text{m}$ . Molybdenum is suited due to its high melting point and low thermal coefficient of expansion  $4.8 \text{ ppm/}^\circ\text{C}$ . The other materials are Silicon, Titanium and Tungsten. Their thermal and mechanical properties are given in tables of the appendix B.



### 3.3 Modeling instruction

We have used Comsol Multiphysics finite element method software for modeling and simulating our MEMS pressure sensor. Starting from pre-existing model in the Comsol models library, we can study different physical phenomena models which are basically coupled, allowing us to be able to account those multiphysics phenomena. In our case, we can further enhance the Comsol simulation platform with dedicated physics interfaces and tools. In this model, we perform an analysis of a sensor design using the electro-mechanics interface. In the coming sections we quote the main instructions to follow in performing the model and the study. In the purpose to compare our device behavior with those of [61-62] we used the same geometric data. As our simulations on the device for different materials are similar we give only one workflow for a given material combination. For remain cases, it was enough to only change the corresponding material input data from the Comsol library or manually from materials data references.

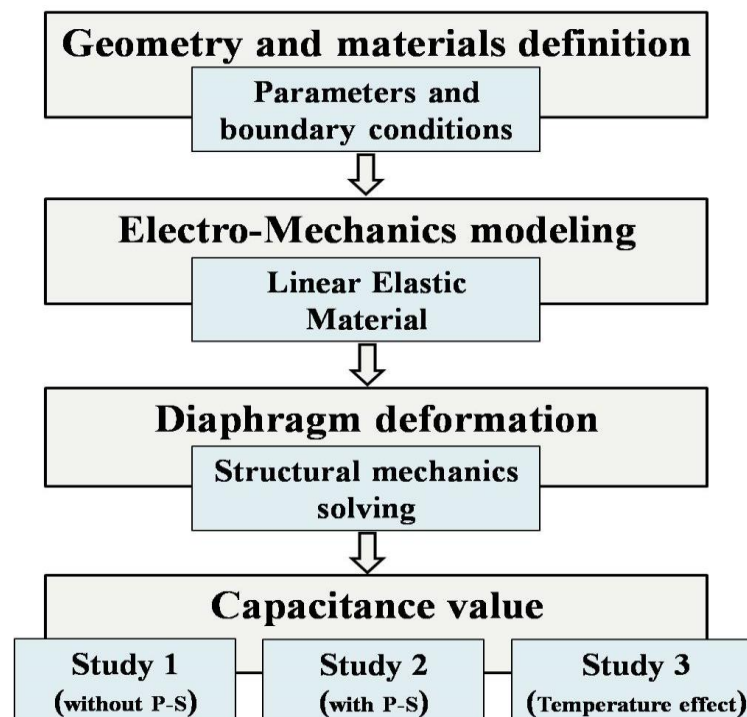


**Figure 3.3:** Diagram flow of Modeling and Numerical Simulation Procedure.

To study the evolution of capacitance value with applied pressure an Electro-mechanics interface (emi) analysis is carried out. The model consists in two coupled parts:

- a) Linear Elastic Material node part to solve the equations of structural mechanics,

- b) Structural mechanics part under EMI interface solved in the sensing element that is the diaphragm.

The entire procedure used is shown as a flow diagram in Fig. 3.3 and discussed below.

The capacitive pressure sensor model is a part of a material die that has been bonded to a metal plate at 70 °C. Since the geometry is symmetric and if symmetry boundary conditions are considered, only a single quadrant of the geometry is included in the model.

The main ideas of our study are

- First the device is considered in the absence of packaging stresses.
- Second the device response at fixed temperature is evaluated in presence of additional packaging stress.
- Finally the temperature dependence of the device response at a fixed applied pressure is assessed.
- Repeat these steps for various materials to optimize the best qualities of the sensor.

### 3.3.1 Model Definition in Comsol Multiphysics

When dealing with modeling under Comsol Multiphysics, the first step is to choose the type of study and the specific interface to generate the model. Since the device has a spatial extension we have also to select the 3D parameter for the dimension. All these are done from the File menu of the COMSOL interface. Our study is independent of time thus we select *Stationary* from preset studies Figure 3.5. The suitable interface in our problem is *Electromechanics (emi)*, thing which permits a structural mechanics analysis Figure 3.4.

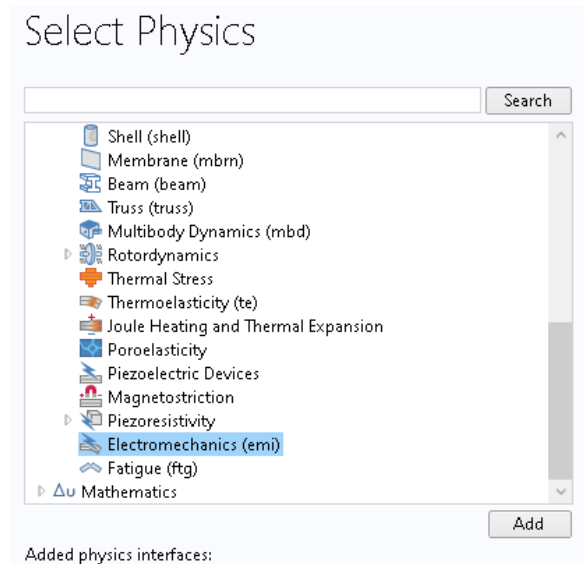


**Figure 3.4 :** Electromechanic Interface of Comsol Multiphysics.

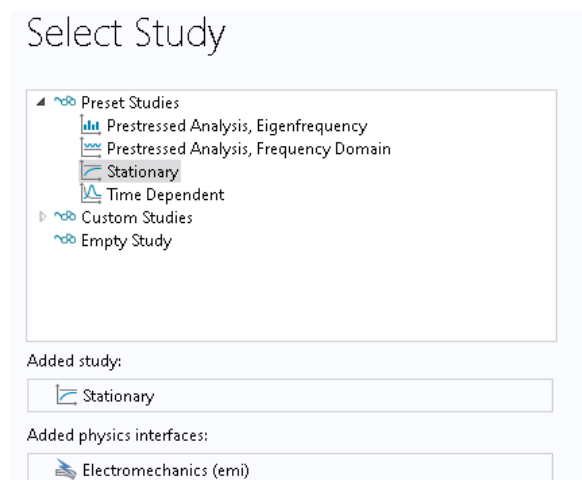


**Figure 3.5:** The Stationary study from the Preset Studies used for the modeling.

### 3.3.2 Geometry

For convenience, the geometry specifications are inserted from an existing file. Instructions for creating the geometry are given in the Appendix A. As said before we keep the same geometry as in [60,61] and the same file name: *capacitive\_pressure\_sensor\_geom\_sequence.mph*.

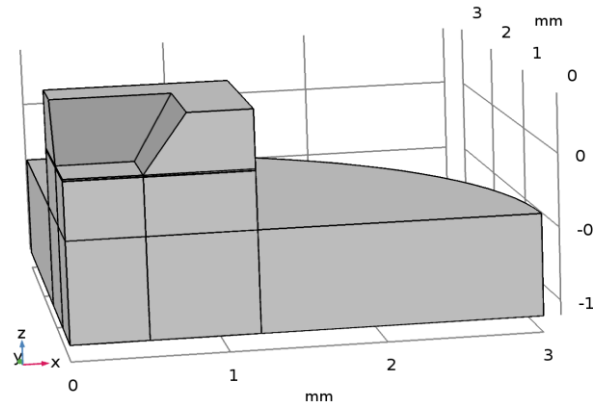


**Figure 3.6:** The sensor geometry

On the Geometry toolbar of the menu, we click *Insert Sequence* to load the above file. After browsing to the model's Application Libraries folder and double-click the file *capacitive\_pressure\_sensor\_geom\_sequence.mph*, we click *Build All* on the Geometry toolbar. In the view panel we will get a structured geometry (Figure 3.6) with the above specifications and the layers of the sensor are labeled as follow just after

Description	Value
<b>Space dimension</b>	3
<b>Number of domains</b>	10
<b>Number of boundaries</b>	54
<b>Number of edges</b>	88
<b>Number of vertices</b>	45
Layer name	Thickness (mm)
<b>Layer 1</b>	0.7
<b>Layer 2</b>	0.397
<b>Layer 3</b>	0.003
<b>Layer 4</b>	0.01

**Table 3.1:** Geometric specifications of the model.

### 3.3.3 GLOBAL DEFINITIONS

Next we specify physical parameters imposed to the model. This concerns pressure, room temperature and Die bonding temperature. From the home toolbars and in the Settings window for Parameters, we enter the required values according to this table

Name	Expression	Value	Description
<b>p0</b>	20[kPa]	2E4 Pa	Pressure
<b>T0</b>	20[degC]	293.2 K	Operating temperature
<b>Tref</b>	70[degC]	343.2 K	Die Bonding temperature

**Table 3.2:** Physical parameters imposed to the model.

In the next section of definitions, we add a component coupling operator to compute a derived global quantity from the model. Comsol's solvers can use these operators during the solution process, for example to include integral quantities in the equation system. This is called Average operator (**aveop1**) and is added to compute the average displacement of the diaphragm. Also, point integration is used to make available the displacement of the center point of the diaphragm (**intop1**). To accomplish this part, on the Definitions toolbar, we click Component Couplings and choose Average and Select Boundary 12 in the Geometric entity level list under Settings window for Average. The boundary 12 is the lower part of the diaphragm Figure 3.7.

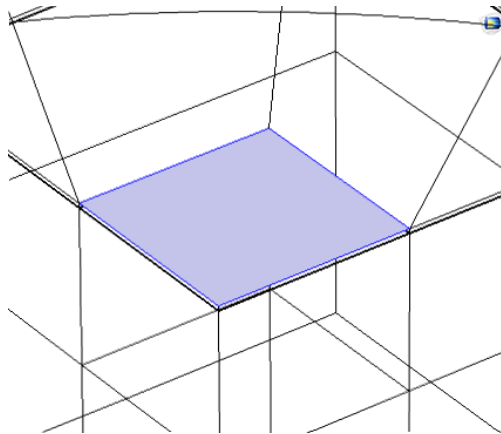


**Figure 3.7 :** The lower face of the diaphragm subject of displacement.

For the integration operator (**intop1**) and on the Definitions toolbar, we select Integration from Component Couplings. Then we select Point 4, situated in center of the boundary 12, from the Geometric entity level list Figure 3.9.

Next, we define selections to simplify the set up of materials and physics. There are three boxes to specify from Definitions toolbar. The first box is named YZ Symmetry Plane Figure 3.8.a. Its purpose is to specify the limit of the x maximum which is set to 1e-6. Also we choose *Entity inside box* as an option in Geometric Entity Level section. The second box named XZ Symmetry Plane is introduced with a maximum in y equal to the same value 1e-6 and an option *Entity inside box* as before Figure 3.8.b. The third box is defined with maximum z of -100[um] and it concerns the Steel base domain.

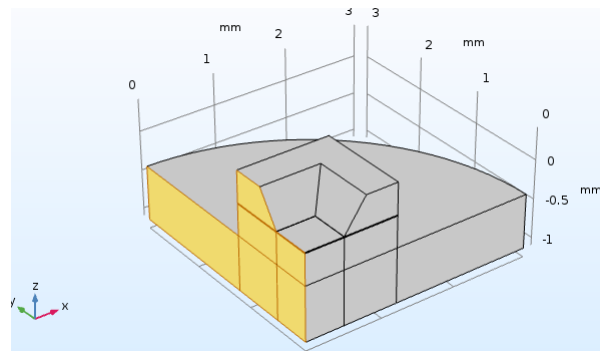


**Figure 3.8.a:** View of the YZ mirror plane.

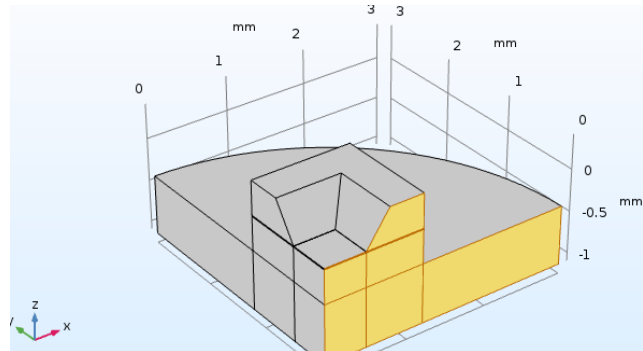


**Figure 3.8.b :** View of the XZ mirror plane.

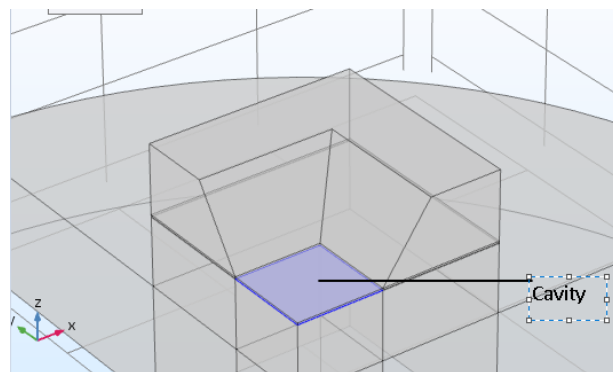


**Figure 3.8.c:** The Cavity of the Sensor (Domain 3)

The next step is to specify explicitly the Cavity (domain 3) and the All domains (1 to 10 but 3 domains) Figure 3.8.c. This is achieved through the usage of the Explicit icon of Definitions toolbar.

The displacement of the cavity is not considered since it does not contain elastic material; it must be subtracted from the simulation. So, we have to add All domains and subtract the Cavity domain. This is done by using the Difference icon on Definitions toolbar followed by checking Add box for All domain and excluding the Cavity domain. This Difference Box carries the name Linear Elastic.

### 3.3.4 ELECTRO-MECHANICS INTERFACE (EMI)

Next, we add the physics settings, such the pressure forces acting on the sensor, the applied sense voltage, and other appropriate boundary conditions. In the Electro-mechanics

Interface, we use a Linear Elastic Material node to solve the equations of structural mechanics only. The electric field is forbidden in all regions but the cavity. In the Model Builder window and under after right-clicking Electro-mechanics (emi) we choose Linear Elastic Material. After, we apply the structural symmetry boundary condition on the symmetry boundaries.

#### Symmetry 1

To duplicate the physics of the first quadrant of the pressure sensor, we use the mirror symmetry (XZ Symmetry Plane) definite in above by choosing the boundary condition Structural>Symmetry which is inserted in the Electro-mechanics node under Model Builder window.

#### Symmetry 2

This symmetry is similar to the first with the exception we choose YZ Symmetry Plane instead of XZ plane. The electrical boundary condition on the charge is applied by default  $q = 0$ . The motion of the device is constrained in most directions by the structural symmetry boundary conditions. However, the whole device can still move up and down along the z-axis. Applying a point constraint will prevent this translation sliding.

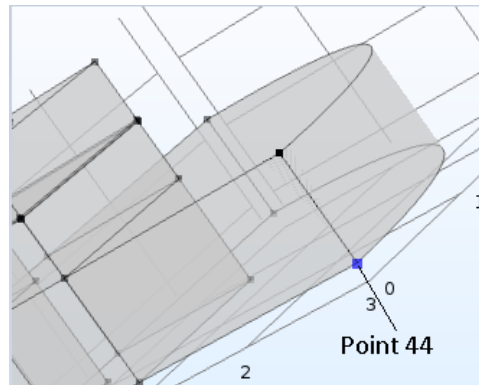


**Figure 3.9** : Definition of the no sliding reference point (44) of the Sensor.

This is done through Prescribed Displacement 2 node where we select Point 44 only Figure 3.9. Prescribed in z direction check box will set 0 to the whole device displacement.

### 3.3.5 BOUNDARY CONDITIONS

Now we apply a Boundary Load, pressure acting on the surface of the diaphragm. By right-clicking Electro-mechanics (emi) and choosing the boundary condition Structural>Boundary Load and selecting Boundary 13, we can insert a value of a force or if we want a pressure. In our case it is the pressure  $p_0$ .

#### a. Moving mesh boundary conditions

These conditions must be applied on borders where the air domain deforms and where the default Electro-mechanical Interface boundary condition does not apply. The Electromechanical Interface boundary condition automatically gets its values from the interface between structural and deforming air domains. It applies the suitable electrical forces to the structural layer and constrains the deformation of the air domain to be equal to that of the structure.


#### b. Prescribed Mesh Displacement 1

By clearing the prescribed z displacement check box we allow the membrane and the mesh to move in the z-direction. This is done in the Settings window for Prescribed Mesh Displacement under the Model Builder window.

#### c. Terminal 1 and Ground 1

Now, let define Terminal and Ground features of the model to apply boundary conditions for the electrostatics parts of the problem. Again by right-clicking Electromechanics node and choosing the boundary condition Electrical>Terminal, we put a Voltage with value 1Volt and apply it to the Boundary 12. Then we select Boundary 9 to be the electrical Ground.

### 3.3.6 Materials

The pressure sensor consists of a specific material die with an enclosed cavity sealed at a low pressure. The pressure sensor is bonded onto a cylindrical plate during the packaging process. The default model uses silicon as predefined material for the plate, but soon we will substitute it for specific material depending on the study and the domain of the device. The cavity also needs 'material' properties  to define the relative permittivity and a user defined material is used to set the relative permittivity to 1 in this region. In the Model Builder window, we add Material from Comsol library. We expand the Built-in node and select Molybdenum which create a selection icon .

The Molybdenum is specified for the 2, 4, 6-9 domains. For remain domains we add the material 2 (Tungsten) in similar way from the library. The third material is inserted in the Cavity (domain 3) manually with a relative permittivity equal to 1; Then, clicking to expand the Material properties section and locate the Material Properties section. From the Material type list, we choose Nonsolid. Right-click Component 1 (comp1)>Materials>Material 3 (mat3) and choose Rename. In the Rename Material dialog box, type in the New label text field. Click OK.



### 3.3.7 The mesh.

The next duty is to set up a structured mesh to solve the problem on. In the Model Builder window, under Component 1 (comp1) we right-click Mesh 1 and choose Edit Physics-Induced Sequence. We disable the default free tetrahedral mesh and we set the Maximum element size of the mesh elements by giving the value 50[um]. We start creating the mesh from boundary 3 as shown in the below Figure 3.10 (Green part)

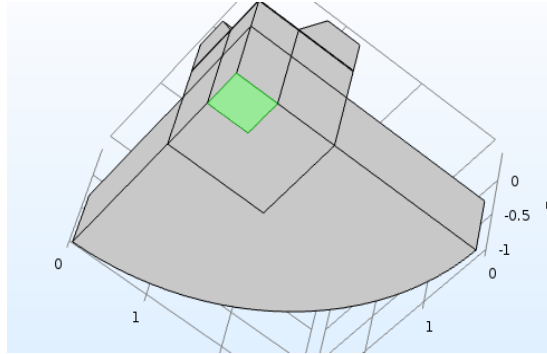


**Figure 3.10:** The starting mesh boundary.

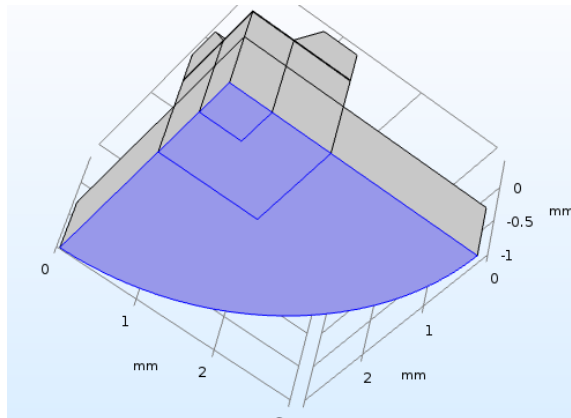


**Figure 3.11 :** The extended mesh surface on the bottom of sensor.

Then we sweep the surface mesh through the structure. This means to extend the boundary 3 to Boundaries 3, 16, and 32 only in the XY plane Figure 3.11. At last, by clicking Built All in the Settings windows for Mapped and Swept we come out with the final mesh given through the 3D structure Figure 3.12.

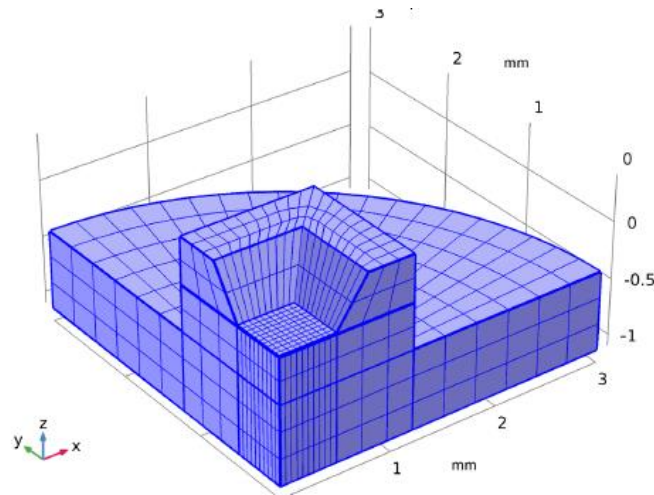


**Figure 3.12** : The final generated mesh.

### 3.4 The capacitive Sensor Studies

The following will set up a study that ranges over a collection of applied pressures, so that the response of the sensor can be evaluated. This study is stationary and pressure starts from  $p_0$ .

#### 3.4.1 STUDY 1(without packaging stress)

In the Model Builder window, we expand the Study 1 node, then click Step 1: Stationary. In the Settings window for Stationary, we Add the Auxiliary sweep checked box. In the Range dialog boxes, we type 0 in the Start text field, 5000 in the Step text field and 20000 in the Stop text field. On the Home toolbar, we execute simulation by clicking Compute.

#### 3.4.2 STUDY 2(with packaging stress)

We add a new study to compute the system response including thermal expansion effects. Indeed, on the Home toolbar, we click Add Study to open the Add Study window in which we find the Studies subsection. In there, we select Preset Studies>Stationary and activate the study and then after we check Auxiliary sweep box under the Study Extensions section of the Settings window for Stationary. The continuation parameter  $p_0$  is added by default. This is the correct parameter to sweep over. In the Range dialog box, we type 0 in the Start text field, 5000 in the step text field and 20000 in the Stop text field. Then we launch the computation.

#### 3.4.3 STUDY 3 (Effect of temperature with Constant pressure)

Now we add a new study to compute the system response including temperature dependence of the capacitance. We don't repeat all steps and instructions of Comsol but we mention that this study is also stationary. We sweep over operating temperature at constant applied pressure, to assess the temperature sensitivity of the device. In the Range dialog

box, we type 290 in the Start text field, 5 in the Step text field and 300 in the Stop text field for temperature. For this study we disable the default plots, as these will be very similar to those already generated by Study 2. At last on the Home toolbar, we click *Compute*. We add a plot to show how the sensor response varies with temperature. The response is computed at an applied pressure set by the value of the parameter  $p_0$ , defined as 20 kPa.

### 3.5 Conclusion

At present, Pressure Sensor are manufactured with several methods and different materials, which will contribute to the diversity of form and function of this device. This model shows the Pressure measurement based on Capacitive effect.

In this chapter, we have defined the concept of the of MEMS capacitive pressure Sensor . This geometry model from a single crystal Molybdenum consists of two parallel plates acting as electrodes of capacitors and separated by air gap, thus forming a square die bonded to a wafer. Subsequently, we will present the operating principle of this sensor, able to provide better Thermal stresses and response of the sensor in order to be able to do its complete design and the possibility of making this device.

## **CHAPTER 4 : RESULTS AND DISCUSSION**

### 4.1 Introduction

Pressure sensors which are our main focus in this thesis, can contain multiple devices for working out many different sorts of detecting and measurement problems to accomplish many tasks with this acquiring sensing data. This is particularly true in all applications where the pressure value must be strictly detected. Therefore, these devices can be included into a printed circuit board or a microchip. They are used for rotational and linear position encoding, liquid level sensing, tactile sensing, sensitive micrometers, digital carpenter's levels, key-switches, light switches and nearness detection. Actually, our phone and tape recorder use microphones with capacitive sensing. Our car's airbag may be deployed by a silicon accelerometer which uses capacitive pressure sensing.

The capacitive sensors can be unaltered by humidity, temperature, or mechanical distortion. They exhibit good screen effect against stray electric fields than inductive sensors which are not easily shielded against magnetic fields. Capacitive transducer accuracy is excellent. The technology of capacitive sensors is easily integrated, and is distancing forward traditional silicon-based transducers using piezo-resistive and piezoelectric effects (especially that expected sensitivity and stability with temperature are ten times better for capacitive sensors). Capacitive sensors consume very little electric power. Many products which implant capacitive encoders have been successful in the market for the above cited reasons.

In this chapter, we comment the results of modeling of the capacitive pressure sensor. For this simulation, we have chosen two materials: the Molybdenum for the head of the sensor (The Die) and Tungsten for the steel plate. In parallel simulations we have made other materials selections, but for the lack of space we do not comment all of them even they present interesting proprieties.

## 4.2 Diaphragm behavior analysis

### 4.2.1 Total displacement study without packaging

The most of the structure is not displaced in this initial study and to facilitate results analysis we will take a selection from the solution to ensure that only the domains of interest will be displayed in the plots. This is done by executing the following sequence in the Model Builder window: expand the Results>Data Sets node, then click Study 1/Solution 1 (sol1). We select Domains 3 and 4 only from the Geometric entity level list. The plot now shows the displacement of the diaphragm only, which has a maximum in the center of the sensor Figure 4.1 (red corner).

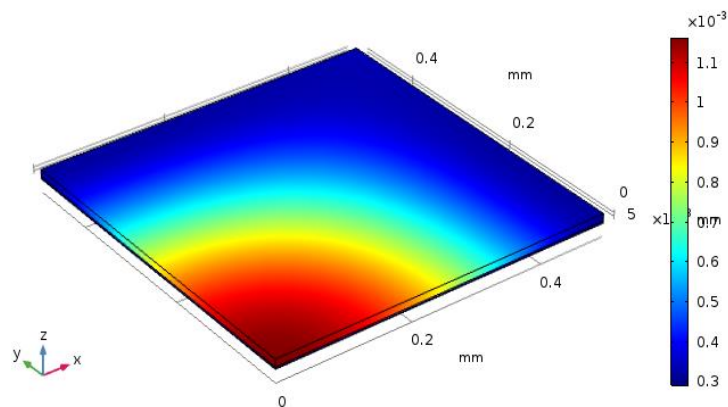


**Figure 4.1:** p0(5)=20000 Surface: Total displacement (mm)

Figure 4.1 shows the deformation of the membrane when a pressure of 20 kPa is applied to it, in the absence of packaging stresses. The reddish part of the square is around the center of the membrane where the deflection is maximal (1.1E-3 mm).

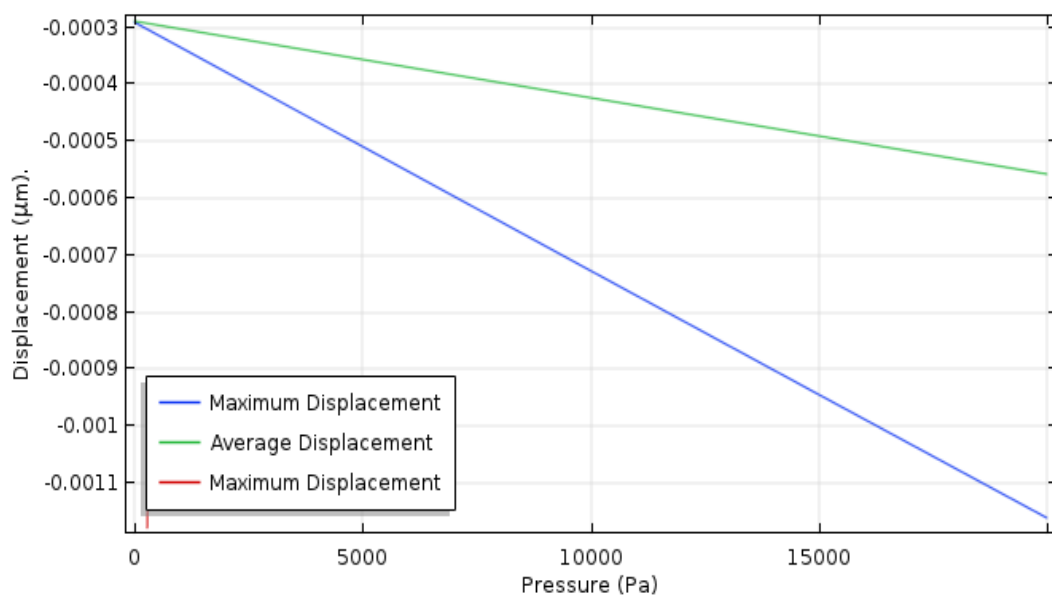


**Figure 4.2:** Maximum and mean displacement of the membrane versus the pressure and without packaging stresses.

Figure 4.2 shows the mean and maximum displacements of the membrane as a function of applied pressure. At an applied pressure of 10 kPa the diaphragm displacement in the center is  $0.73 \mu\text{m}$ . The average displacement of the diaphragm is  $0.42 \mu\text{m}$ .

#### 4.2.2 Total displacement study with packaging

At an applied pressure of 10 kPa and in presence of packaging stresses the diaphragm displacement in the centre is  $0.95 \mu\text{m}$ . The average displacement of the diaphragm is  $0.43 \mu\text{m}$ . Notice that at pressure 0 the diaphragm has a displacement of  $0.8 \mu\text{m}$  resulting from packaging stresses. In general the operating device is calibrated to avoid this displacement in the experimental measure processes. Also we have to notice the diaphragm displacement sensibility is less in the case of packaging stresses than in unstressed case Figure 4.3.

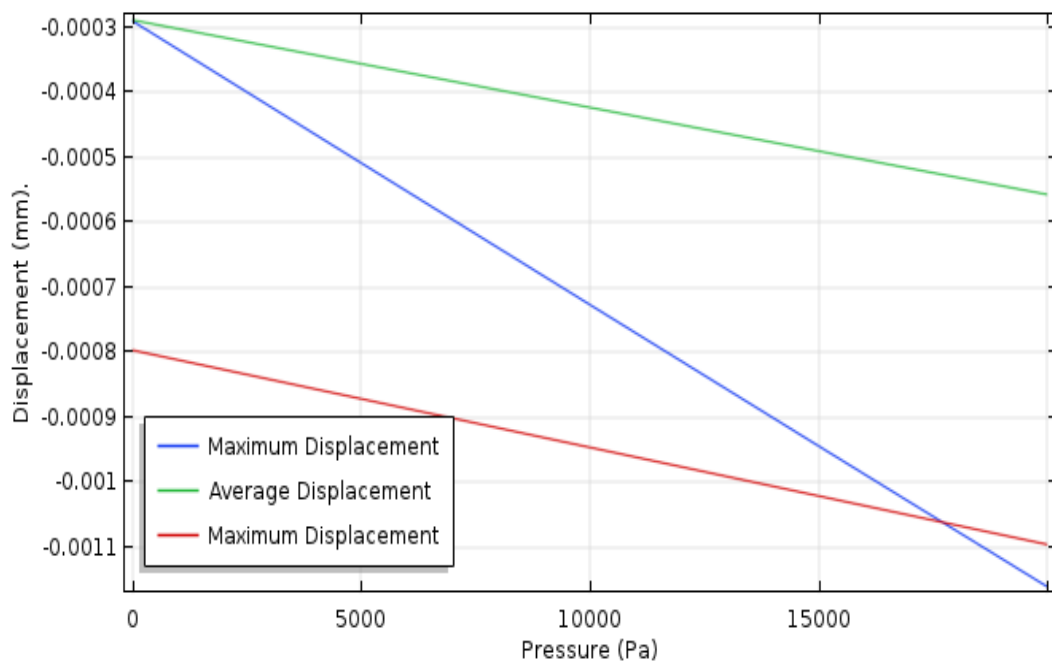


**Figure 4.3:** Diaphragm displacement (red curve) with packaging stresses. The green and blue curves are for unstressed device.

#### 4.2.3 Electrical potential study

Figure 4.4 shows the potential on a plane located between the two plates of the sensor. The deformation of the membrane is of the form estimated, and results in a non-uniform potential between the plates.

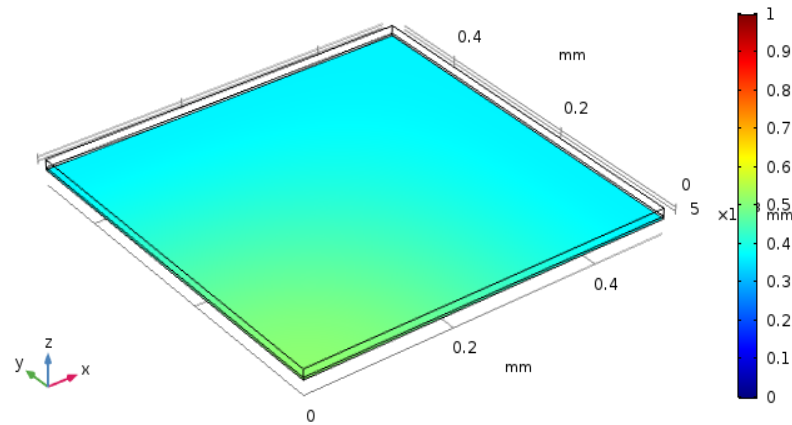


**Figure 4.4:** Electric potential in the cavity of the capacitive sensor.

### 4.3 Capacitance response discussion

#### 4.3.1 Capacitance versus pressure

Now, we show the plot of the sensor capacitance as a function of the applied pressure. Since the Terminal boundary condition was used for the underside of the diaphragm, COMSOL automatically computes its capacitance with respect to ground. The value of the capacitance is available as a variable in results analysis. The same steps, as done for the previous plot, will give the plot of Figure 4.5 with the x-axis and y-axis labeled respectively Pressure (Pa) and Capacitance (pF). Finally, we had given as plot name ‘Model Capacitance vs Pressure’ in the New label text field. Next, we had add thermal expansion to evaluate the effects of packaging stresses on the device performance.

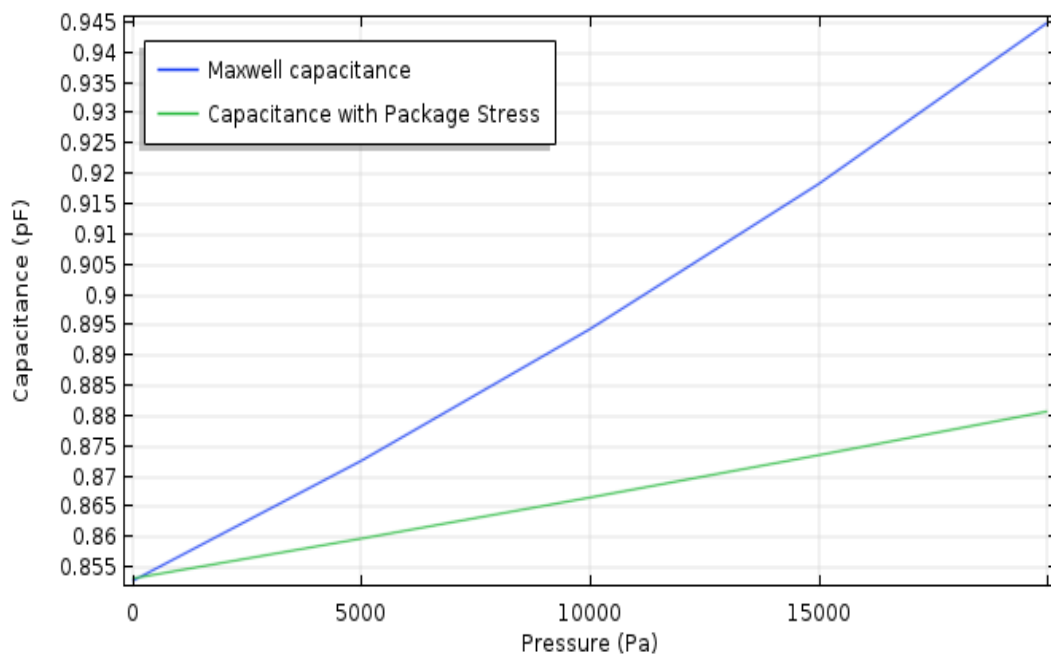


**Figure 4.5:** Capacitance versus pressure, with and without the packaging stresses.

Figure 4.5 shows that the capacitance of the device increases linearly with applied pressure. The gradient of the curve plotted is a measure of the sensitivity of the sensor. The sensitivity of the model (1/4 of the whole sensor) is  $4.6 \times 10^{-6}$  pF/Pa. The device sensitivity is therefore  $18.4 \times 10^{-6}$  pF/Pa.

Let compare the plot of Figure 4.5 with those using Steel AISI 4340 (in the plate) and Silicon in the die Figure 4.6 [62] which we have also reproduced by Comsol. The response of the device with the additional packaging stresses is shown in this figure. At zero applied pressure the sensitivity of the COMSOL model has increased from  $6.5 \times 10^{-6}$  pF/Pa to  $10 \times 10^{-6}$  pF/Pa. The effect is even more important at a pressure of 20 kPa, where the model with thermal stresses exhibit a pressure sensitivity of  $25 \times 10^{-6}$  pF/Pa compared to the unstressed case. The sensitivity of the device to pressure has doubled and a dependence on temperature has been introduced into the device response. Since the thermal stresses are temperature dependent, the response of the device is also temperature dependent. The model shows the importance of carefully considering the packaging in the MEMS design process.

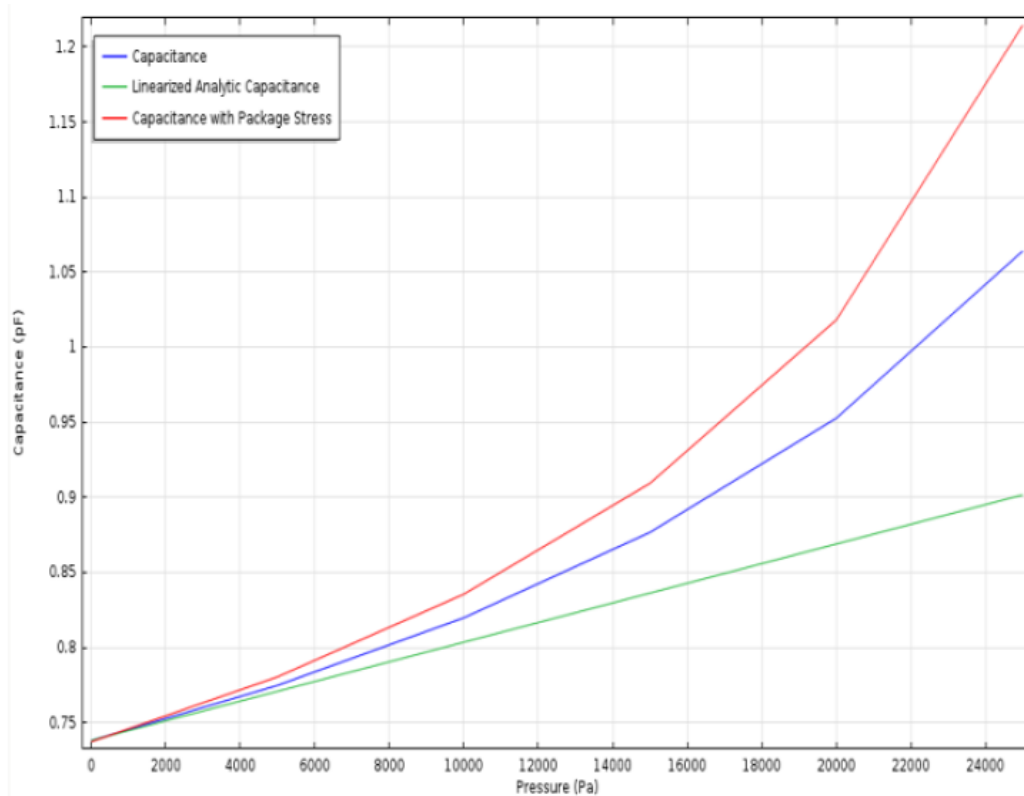


**Figure 4.6:** Capacitance vs. Pressure for square diaphragm with packaging stress [62].

Next the response of the device is studied when packaging stresses are present in the model. For this part it is assumed that the device is operated at  $20^\circ\text{C}$  and that the system



was stress and displacement free at the bonding temperature (70°C). Figure 4.7 shows the displacement of the structure at the room temperature operating point, with an applied pressure of 20 kPa. Notice that the entire structure is now displaced at room temperature as a result of thermal expansion.

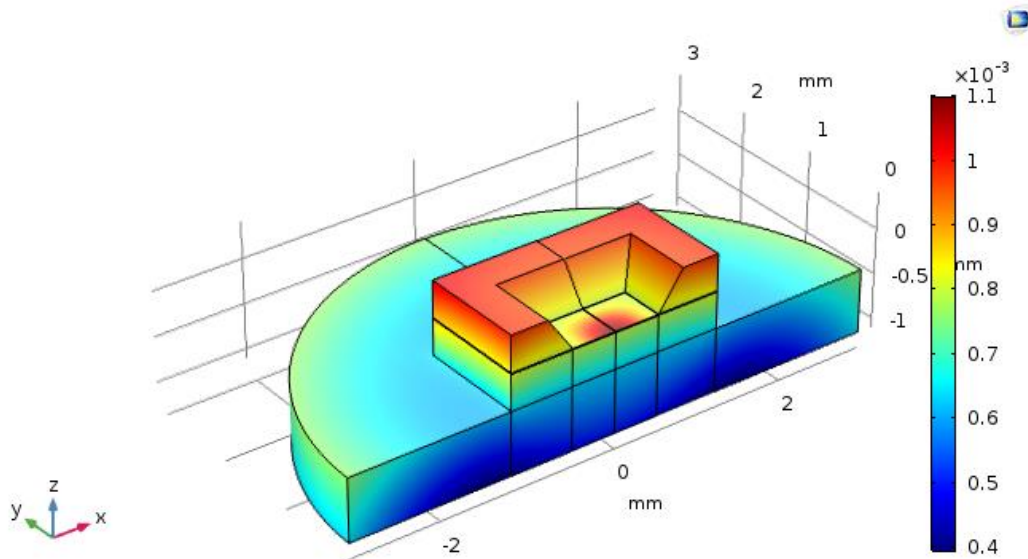


**Figure 4.7:** The displacement (pressure of 20 kPa) with packaging stresses.

The complex interaction between the thermal stresses and the stresses introduced as a result of the applied pressure has resulted in both the initial offset displacement and the increased dependence of the displacement on the pressure.

#### 4.3.2 Capacitance versus operating temperature

In the Electromechanics (emi) interface we had chosen Thermal Expansion for Linear Elastic Material 1. The model temperature was set to the previously defined room temperature parameter, T0. The reference temperature indicates the temperature at which the structure had no thermal strains. In this case, we had set it to the previously defined parameter, Tref, which represents the temperature at which the die material was bonded to the ground plate. Thus, we located the Thermal Expansion Properties section and in the Tref text field, we typed Tref. The user defined properties, we added previously for Molybdenum, include its thermal expansion coefficient.

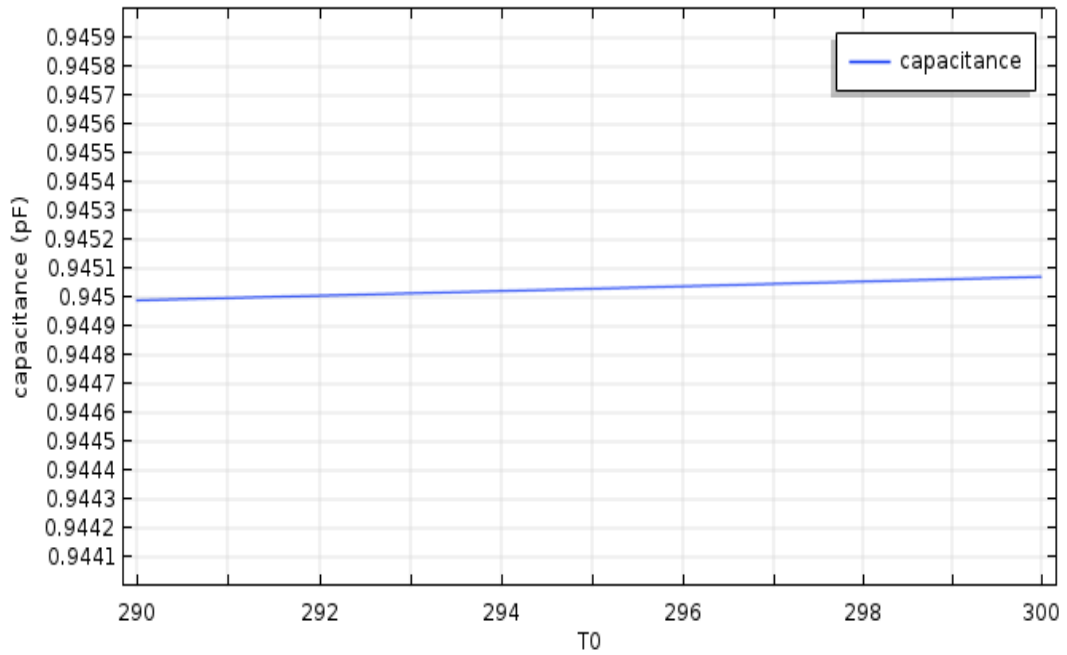


**Figure 4.8:** Capacitance versus temperature.

In this figure the temperature dependence of the capacitance of device is shown. The capacitance varies slightly with temperature in the ranges [290,300].

#### 4.4 Sensitivity analysis of capacitive pressure sensors

In this section the sensitivities of the different plots are shown below. For every plot the sensitivity is computed by the slope of the tangent to the curve at a given abscisse value. As all the plots are linear, the sensitivity is the same along the horizontal axis. The following Table 4.1 summarizes the sensitivities of the studied capacitive pressure sensor, both the quadrant and the whole device (values given in bold). This model shows that a thermal independence of the capacitive pressure sensor made of Tungsten and Molybdenum. Notice that the packaging as in above has no effect on sensor performance. Notice also that even the small the temperature sensitivity is the slope of the curve is positive which is different from the temperature sensitivity of reference [62].

	Without packaging Stresses	With packaging Stresses
Displacement pressure sensitivity (um/Pa)	4.36 x 10 <sup>-4</sup> <b>17.46 x 10<sup>-4</sup></b>	1.49 x 10 <sup>-4</sup> <b>5.98 x 10<sup>-4</sup></b>
Capacitance pressure sensitivity (pF/Pa)	4.35 x 10 <sup>-6</sup> <b>17.40 x 10<sup>-6</sup></b>	1.35 x 10 <sup>-6</sup> <b>5.41 x 10<sup>-6</sup></b>
Temperature capacitance sensitivity (pF/K) with a fixed pressure $P = 20$ kPa.		8.2 x 10 <sup>-6</sup> <b>5.41 x 10<sup>-6</sup></b>

**Table 4.1:** The sensitivities of the studied capacitive pressure sensor.

#### 4.5 Conclusion

In this last chapter, we presented the hypotheses considered to develop this capacitive pressure sensor model. Next, we have detailed the sensitivity of the sensor and its performance compared to other references. Then, the simulation results obtained on the micrometric scale using a single crystal Molybdenum materials were analyzed and discussed, to validate this model, using the Electro-Mechanics interface (EMI).

From this study, we conclude that the diaphragm deflection and the increase in temperature are two essential factors for measuring of pressure from the capacitance variation. The increase in temperature influences on our MEMS pressure sensor. Then the sensitivity of capacitive pressure sensor change with and without packaging stress.

## GENERAL CONCLUSION

A MEMS pressure sensor or pressure microsensor Based on Capacitive Effect is very small dimensions device less than 1 mm in which can contain many sorts of detecting and measurement problems. It is manufactured using different methods and materials. Therefore, these devices can be included into a printed circuit board or a microchip. The study of plate mechanical deflection in these devices calls on various notions of solid mechanics and electrical potential grouped together under the name of electro-mechanics in connection with the applied pressure. The principle of using these devices is relatively simple. It is based on two parallel plates acting as electrodes of capacitors and separated by air gap, thus forming a square diaphragm. When the pressure over the sealed cavity changes the pressure difference causes the membrane to deflect. This sensor is able to provide better Thermal stresses and response in order to be able to do its complete design and the possibility of making this device.

In a first step, we have introduced a state of the art of capacitive pressure sensors. Next, we presented some aspects as well as applications and the mathematical techniques of Finite Elements Methods (FEM) and some material used in this work. Subsequently, we proposed and presented the detailed description of the model concept, its operating principle of the device, the geometry of the sensors and simulations of pressure and thermal effects as well as its diagram flow for the possibility of carrying out these measures. Therefore, we discuss the results of the simulation and have focused on the sensibility of the pressure capacitive sensor and its performance compared to other references.

Through this work, we relied on finite element simulations and studies using the Comsol Multiphysics software, an interesting type of MEMS sensors called capacitive pressure sensors which convert pressure signal into induced potential difference with high sensibility. We conclude that the diaphragm deflection, the increase in temperature and the pressure effects are essential factors for the operational objective of this system. These factors influences on: (i) The capacitance of MEMS device and (ii) Its sensitivity (the gradient of the curve Capacitance Vs Pressure ). Also, we have examined the packaging effect on the two preceding points. And at last we have plotted the behavior of capacitance under temperature variation in the working range 290 to 300 K°. The stability of the device

in this case was an excellent result attempted by manufacturing processes. Molybdenum simulations results are quoted in the final results in this thesis.

There are immense prospects in the field of microsensors for pressure measurement being used in engineering and laboratories. We plan to further explore the design aspect of this system and the possibility of improving its performance at higher temperatures and lower pressure with other less expensive materials in order to optimize the cost of realization. Also, the next step will be the realization of an experimental prototype of this pressure sensor Based on capacitive effect in order to proceed to its characterization and its final validation for its use.

## APPENDIX A Geometry Instructions

From the File menu, choose New.

### NEW

In the New window, click Blank Model.

### ROOT

On the Home toolbar, click Component and choose Add Component>3D.

### Geometry 1

1. In the Model Builder window, under Component 1 (comp1) click Geometry 1.
2. In the Settings window for Geometry, locate the Units section.
3. From the Length unit list, choose mm.

### Block 1 (blk1)

1. On the Geometry toolbar, click Block.
2. In the Settings window for Block, locate the Size and Shape section.
3. In the Width text field, type 1.2.
4. In the Depth text field, type 1.2.
5. In the Height text field, type 1.51.
6. Locate the Position section. In the z text field, type -1.1.
7. Click to expand the Layers section. In the table, enter the following settings:

Layer name	Thickness(mm)
<b>Layer 1</b>	0.7
<b>Layer 2</b>	0.397
<b>Layer 3</b>	0.003
<b>Layer 4</b>	0.01

**Table A.1:** Layers thickness of the CPC.

### Block 2 (blk2)

1. On the Geometry toolbar, click Block.
2. In the Settings window for Block, locate the Size and Shape section.
3. In the Width text field, type 0.5.

4. In the Depth text field, type 0.5.
5. In the Height text field, type 1.51.
6. Locate the Position section. In the z text field, type -1.1.

#### Partition Domains 1 (pard1)

1. On the Geometry toolbar, click Booleans and Partitions and choose Partition Domains.
2. On the object blk1, select Domains 1–4 only.
3. In the Settings window for Partition Domains, locate the Partition Domains section.
4. From the Partition with list, choose Objects.
5. Select the object blk2 only.

#### Hexahedron 1 (hex1)

1. On the Geometry toolbar, click More Primitives and choose Hexahedron.
2. In the Settings window for Hexahedron, locate the Vertices section.
3. In row 2, set x to 0.5.
4. In row 3, set x to 0.5.
5. In row 4, set x to 0.
6. In row 6, set x to 0.78322.
7. In row 7, set x to 0.78322.
8. In row 8, set x to 0.
9. In row 2, set y to 0.
10. In row 3, set y to 0.5.
11. In row 4, set y to 0.5.
12. In row 6, set y to 0.
13. In row 7, set y to 0.78322.
14. In row 8, set y to 0.78322.
15. In row 1, set z to 0.01.
16. In row 2, set z to 0.01.
17. In row 3, set z to 0.01.
18. In row 4, set z to 0.01.
19. In row 5, set z to 0.41.
20. In row 6, set z to 0.41.
21. In row 7, set z to 0.41.
22. In row 8, set z to 0.41.

#### Difference 1 (dif1)

1. On the Geometry toolbar, click Booleans and Partitions and choose Difference.
2. Select the object pard1 only.
3. In the Settings window for Difference, locate the Difference section.
4. Find the Objects to subtract subsection. Select the Active toggle button.
5. Select the object hex1 only.

#### Cylinder 1 (cyl1)

1. On the Geometry toolbar, click Cylinder.
2. In the Settings window for Cylinder, locate the Size and Shape section.
3. In the Radius text field, type 3.
4. In the Height text field, type 0.7.
5. Locate the Position section. In the z text field, type -1.1.

#### Partition Domains 2 (pard2)

1. On the Geometry toolbar, click Booleans and Partitions and choose Partition Domains.
2. On the object cyl1, select Domain 1 only.
3. In the Settings window for Partition Domains, locate the Partition Domains section.
4. From the Partition with list, choose Extended faces.
5. On the object dif1, select Boundaries 17 and 38 only.
6. In the tree, select dif1.
7. Click Build Selected.
8. On the Geometry toolbar, click Delete.

#### Delete Entities 1 (del1)

1. In the Model Builder window, under Component 1 (comp1)>Geometry 1 click

#### Delete Entities 1 (del1).

2. In the Settings window for Delete Entities, locate the Entities or Objects to Delete section.
3. From the Geometric entity level list, choose Domain.
4. On the object pard2, select Domains 1–3 only.
5. On the object blk2, select Domain 1 only.

#### Form Union (fin)

1. In the Model Builder window, under Component 1 (comp1)>Geometry 1 click Form Union (fin).
2. In the Settings window for Form Union/Assembly, click Build Selected.

#### Explicit Selection 1 (sel1)



1. On the Geometry toolbar, click Selections and choose Explicit Selection.
2. In the Settings window for Explicit Selection, type YZ Symmetry Plane in the Label text field.
3. Locate the Entities to Select section. From the Geometric entity level list, choose Boundary.
4. Select the Group by continuous tangent check box.
5. On the object fin, select Boundaries 1, 4, 7, 10, 14, 17, 20, 23, 26, and 30 only.

#### Explicit Selection 2 (sel2)

1. On the Geometry toolbar, click Selections and choose Explicit Selection.
2. In the Settings window for Explicit Selection, type XZ Symmetry Plane in the Label text field.
3. Locate the Entities to Select section. From the Geometric entity level list, choose Boundary.
4. Select the Group by continuous tangent check box.
5. On the object fin, select Boundaries 2, 5, 8, 11, 40, 42, 44, 46, 48, and 50 only.

#### Box Selection 1 (boxsel1)

1. On the Geometry toolbar, click Selections and choose Box Selection.
2. In the Settings window for Box Selection, type Steel Base in the Label text field.
3. Locate the Box Limits section. In the z maximum text field, type -0.1.
4. Locate the Output Entities section. From the Include entity if list, choose Entity inside box.

#### Explicit Selection 3 (sel3)

1. On the Geometry toolbar, click Selections and choose Explicit Selection.
2. In the Settings window for Explicit Selection, type Cavity in the Label text field.
3. On the object fin, select Domain 3 only.

#### Explicit Selection 4 (sel4)

1. On the Geometry toolbar, click Selections and choose Explicit Selection.
2. In the Settings window for Explicit Selection, type Geometry in the Label text field.
3. Locate the Entities to Select section. From the Geometric entity level list, choose Object.
4. Select the object fin only.

#### Difference Selection 1 (difsel1)

1. On the Geometry toolbar, click Selections and choose Difference Selection.

2. In the Settings window for Difference Selection, type Linear Elastic in the Label text field.
3. Locate the Input Entities section. Click Add.
4. In the Add dialog box, select Geometry in the Selections to add list. Click OK.
5. In the Settings window for Difference Selection, locate the Input Entities section. Click Add.
6. In the Add dialog box, select Cavity in the Selections to subtract list. Click OK.

**APPENDIX B**  
**Proprieties tables of MEMS materials**

B.1 Silicon:

<b>Atomic number of Si</b>	14	<b>Group 3; Period: 3</b>
<b>Atomic mass per isotope of Si</b>	28 (92.23%)	29 (4.67%), 30 (3.1%)
<b>Electronic structure</b>	[Ne] 3s <sup>2</sup> 3p <sup>2</sup>	<sup>3</sup> P <sub>0</sub> (Ioniz. Energy 8.1517 eV)
<b>Crystal structure</b>	Diamond cubic	
<b>Lattice constant</b>	0.5431	Nm
<b>Si atoms</b>	5x10 <sup>22</sup>	Atoms.cm <sup>-3</sup>
<b>Melting point</b>	1687	K°
<b>Boiling point</b>	3538	C°
<b>Specific density</b>	2.329	g.cm <sup>-3</sup> at 298 K
<b>Specific density (liquid)</b>	2.57	g.cm <sup>-3</sup>
<b>Thermal conductivity</b>	149	W.m <sup>-1</sup> K <sup>-1</sup>
<b>Coefficient of thermal expansion</b>	2.56x10 <sup>-6</sup>	m <sup>-1</sup> K <sup>-1</sup> (at 298 K)
<b>Specific heat capacity</b>	19.79	J*mol <sup>-1</sup> K <sup>-1</sup>
	0.705	J*g <sup>-1</sup> K <sup>-1</sup>
<b>Young's modulus</b>	150	GPa
<b>Poisson ratio</b>	0.	
<b>Speed of sound</b>	8433	m*s <sup>-1</sup>
<b>Volumetric compression coefficient</b>	1.02x10 <sup>-8</sup>	kPa <sup>-1</sup>
<b>Index of refraction (varies with temperature and λ)</b>	~3.54 ~3.48	

**Table B.1:** Physical proprieties of Silicon.

B.2 Molybdenum

<b>Atomic number of Mo</b>	42	<b>Group: 6, Period: 5</b>
<b>Atomic mass per isotope of Mo</b>	95.95 ( xx %)	
<b>Electronic structure</b>	[Kr] 4d <sup>5</sup> 5s	<sup>7</sup> S <sub>3</sub> (Ioniz. Energy 7.0924 eV)
<b>Crystal structure</b>	Body centered cubic.	

<b>Lattice constant</b>		Nm
<b>Mo atoms</b>	$5 \times 10^{22}$	Atoms.cm <sup>-3</sup>
<b>Melting point</b>	2896	K°
<b>Boiling point</b>	4912	K°
<b>Specific density</b>	10.28	g.cm <sup>-3</sup> at 298 K
<b>Specific density (liquid)</b>	9.33	g.cm <sup>-3</sup>
<b>Thermal conductivity</b>	138	W.m <sup>-1</sup> K <sup>-1</sup>
<b>Coefficient of thermal expansion</b>	$4.8 \times 10^{-6}$	m <sup>-1</sup> K <sup>-1</sup> (at 298 K)
<b>Specific heat capacity</b>	24.06	J.mol <sup>-1</sup> K <sup>-1</sup>
<b>Young's modulus</b>	329	GPa
<b>Poisson ratio</b>	0.31	
<b>Speed of sound</b>	5400	m.s <sup>-1</sup>
<b>Volumetric compression coefficient</b>		kPa <sup>-1</sup>
<b>Index of refraction (varies with temperature and <math>\lambda</math>)</b>	~ ~	

**Table B.2:** Physical proprieties of Molybdenum.

### B.3 Tungsten [64]

<b>Atomic number of Mo</b>	74	<b>Group: 6, Period: 6</b>
<b>Atomic mass per isotope of Mo</b>	183.8.a5 ( xx %)	
<b>Electronic structure</b>	[Xe] 4f <sup>14</sup> 5d <sup>4</sup> 6s <sup>2</sup>	<sup>5</sup> D <sub>0</sub> (Ioniz. Energy 1st: 770KJ/mol)
<b>Crystal structure</b>	Body centered cubic.	
<b>Lattice constant</b>		Nm
<b>W atoms</b>	$9.39 \times 10^{22}$	Atoms.cm <sup>-3</sup>
<b>Melting point</b>	3695	K°
<b>Boiling point</b>	6203	K°
<b>Specific density</b>	19.3	g.cm <sup>-3</sup> at 298 K
<b>Specific density (liquid)</b>	17.6	g.cm <sup>-3</sup>
<b>Thermal conductivity</b>	173	W.m <sup>-1</sup> K <sup>-1</sup>
<b>Coefficient of thermal expansion</b>	$4.5 \times 10^{-6}$	m <sup>-1</sup> K <sup>-1</sup> (at 298 K)
<b>Specific heat capacity</b>	24.27	J.mol <sup>-1</sup> K <sup>-1</sup>
<b>Young's modulus</b>	411	GPa
<b>Poisson ratio</b>	0.28	
<b>Speed of sound</b>	4620	m.s <sup>-1</sup>

**Table B.3:** Physical proprieties of Tungsten.

## REFERENCES

1. I. Fujimasa: *Micro-machines: A New Era in Mechanical Engineering* (Oxford Univ. Press, Oxford 1996)
2. B. Bhushan: *Tribology Issues and Opportunities in MEMS* (Kluwer, Dordrecht 1998)
3. G. T. A. Kovacs: *Micro-machined Transducers Sourcebook* (WCB McGraw-Hill, Boston 1998)
4. S. D. Senturia: *Micro-system Design* (Kluwer, Boston 2001)
5. T. R. Hsu: *MEMS and Microsystems* (McGraw-Hill, Boston 2002)
6. M. Madou: *Fundamentals of Micro-fabrication: The Science of Miniaturization*, 2nd edn. (CRC, Boca Raton 2002).
7. B. Bhushan: *Tribology and Mechanics of Magnetic Storage Devices*, 2nd edn. (Springer, New York 1996.)
8. H. Hamilton: Contact recording on perpendicular rigid media, *J. Mag. Soc. Jpn.* **15** (Suppl. S2) (1991) 481–483
9. T. Ohwe, Y. Mizoshita, S. Yonoeka: Development of integrated suspension system for a nanoslider with an MR head transducer, *IEEE Trans. Magn.* **29** (1993) 3924–3926.
10. D. K. Miu, Y. C. Tai: Silicon micro-machined scaled technology, *IEEE Trans. Industr. Electron.* **42** (1995) 234–239
11. L. S. Fan, H. H. Ottesen, T. C. Reiley, R.W.Wood: Magnetic recording head positioning at very high track densities using a micro-actuator-based, two-stage servo system, *IEEE Trans. Ind. Electron.* **42** (1995) 222–233
12. D. A. Horsley, M. B. Cohn, A. Singh, R. Horowitz, A. P. Pisano: Design and fabrication of an angular micro-actuator for magnetic disk drives, *J. Micro-electromech. Syst.* **7** (1998) 141–148
13. T. Hirano, L. S. Fan, D. Kercher, S. Pattanaik, T. S. Pan: HDD tracking micro-actuator and its integration issues, *Proc. ASME Int. Mech. Eng. Congress, MEMS*, New York 2000, ed. by A. P. Lee, J. Simon, F. K. Foster, R. S. Keynton (ASME, New York 2000) 449–452
14. [https://www.preciseley.com/uploads/1/7/3/3/17338281/2d-array-op1-copy\\_orig.jpg](https://www.preciseley.com/uploads/1/7/3/3/17338281/2d-array-op1-copy_orig.jpg)

15. Springer Handbook of Nanotechnology, Bharat Bhushan Editor (2004)
16. Y. Wang, M. Esashi: A novel electrostatic servo capacitive vacuum sensor, Technical Digest, IEEE Int. Conf. Solid-State Sens. Actuators, Chicago 1997 (Transducers Conference, Chicago 1997) 1457–1460
17. W. H. Ko, Q. Wang: Touch mode capacitive pressure sensors, Sens. Actuators 75 (1999) 242–251
18. T.A. Core, W.K. Tsang, S.J. Sherman: Fabrication technology for an integrated surface micro-machined sensor, Solid State Technol. 36(10) (1993) 39–47
19. H. Kapels, R. Aigner, C. Kolle: Monolithic surface micro-machined sensor system for high pressure applications, Technical Digest, Int. Conf. Solid-State Sens. Actuators, Munich 2001 (Transducers Conference, Chicago 2001) 56–59
20. Haus, H.A. 1989. Electromagnetic Fields and Energy. Englewood Cliffs, N J" Prentice-Hall., p.66.
21. Southwell, R.V. (1946). Relaxation Methods in Theoretical Physics, Clarendon Press, Oxford, U.K.
22. Ikegawa and Washizu, Finite element method applied to analysis of flow over a spillway crest, <https://doi.org/10.1002/nme.1620060204>
23. Roache , On artificial viscosity, [https://doi.org/10.1016/0021-9991\(72\)90058-7](https://doi.org/10.1016/0021-9991(72)90058-7)
24. Argyris, J.H. (1954). Recent Advances in Matrix Methods of Structural Analysis, Pergamon Press, Elmsford, NY.
25. Turner, M., Clough, R.W., Martin, H., and Topp, L. (1956). Stiffness and deflection of complex structures, J. Aero Sci., 23, 805–823.
26. Clough, R.W. (1960). finite element method in plane stress analysis, in Proceedings of the Second Conference on Electronic Computation, ASCE, Pittsburgh, PA, pp. 345–378.
27. Zienkiewicz, O.C. and Cheung, Y.K. (1965). Finite elements in the solution of field problems, The Engineer, 220, 507–510.
28. Oden, J.T. (1972). Finite Elements of Nonlinear Continua, McGraw-Hill Book Publishers, New York.
29. Huebner, K.H. (1975). Finite Element Method for Engineers, John Wiley & Sons, New York.
30. Heuser, J. (1972). Finite element method for thermal analysis, NASA Technical Note TN\_D-7274, Goddard Space Flight Center, Greenbelt, MD.

31. Baker, A.J. (1971). A finite element computational theory for the mechanics and thermodynamics of a viscous compressible multi-species fluid, Bell Aerospace Research Department 9500-920200.
32. Finlayson, B.A. (1972). The Method of Weighted Residuals and Variational Principles, Academic Press, New York.
33. Desai, C.S. (1979). Elementary Finite Element Method, Prentice-Hall, Inc., Englewood Clis, NJ.
34. Becker, E.G., Carey, G.F., and Oden, J.T. (1981). Finite Elements, An Introduction, Vol. I, Prentice-Hall, Inc., Englewood Clis, NJ.
35. Baker, A.J. (1983). Finite Element Computational Fluid Mechanics, Hemisphere Publishing Corporation, Washington, DC.
36. Fletcher, C.A.J. (1984). Computational Galerkin Methods, Springer-Verlag, New York.
37. Reddy, J.N. (1984). An Introduction to the Finite Element Method, McGraw-Hill Book Company, New York.
38. Segerlind, L.J. (1984). Applied Finite Element Analysis, John Wiley & Sons, New York.
39. Bickford, W.B. (1990). A First Course in the Finite Element Method, Richard D. Irwin, Inc., Homewood, IL.
40. Zienkiewicz, O.C. and Taylor, R.L. (1989). The Finite Element Method, 4th Ed., McGraw Hill Book Company, Maidenhead, U.K.
41. Johnson, C. (1987). Numerical Solution of Partial Differential Equations by the Finite Element Method, Cambridge University Press, Cambridge, U.K.
42. Smith, I.M. (1982). Programming the Finite Element Method, John Wiley & Sons, New York.
43. Owen, D.R.J. and Hinton, E. (1980). A Simple Guide for Finite Elements, Pineridge Press Limited, Swansea, U.K.
44. Rayleigh, J.W.S. (1877). Theory of Sound, 1st Revised Ed., Dover Publishers, New York.
45. Ritz, W. (1909). Über eine Neue Methode zur Lösung Gewisser Variations-Probleme der Mathematischen Physik, J. Reine Angew. Math., 135, 1–61.
46. Chandrupatla, T.R. and Belegundu, A.D. (2002). Introduction to Finite Elements in Engineering, Prentice Hall, Upper Saddle River, NJ.
47. Liu, G.R. and Quek, S.S. (2003). The Finite Element Method: A Practical Course, Butterworth-Heinemann, Boston, MA.

48. Hollig, K. (2003). Finite Elements with B-Splines, Society of Industrial and Applied Mathematics, Philadelphia, PA.
49. Bohn, R.B. and Garboczi, E.J. (2003). User Manual for Finite Element and Finite Difference Programs: A Parallel Version of NISTIR-6269, NIST, Gaithersburg, MD.
50. Hutton, D.V. (2004). Fundamentals of Finite Element Analysis, McGraw-Hill, Boston, MA.
51. Solin, P., Segeth, K., and Dolezel, I. (2004). Higher-Order Finite Element Methods, Chapman and Hall/CRC, Boca Raton, FL.
52. Reddy, J.N. (2006). An Introduction to the Finite Element Method, 3rd Ed., McGraw Hill, New York.
53. Becker, A.A. (2004). An Introductory Guide to Finite Element Analysis, ASME Press, New York.
54. Ern, A. and Guermond, J.-L. (2004). Theory and Practice of Finite Elements, Springer-Verlag, New York.
55. MATHCAD 15. (2014). User's Guide, MathsoEngineering & Education, Inc., Cambridge, MA.
56. MAPLE 18. (2014). Learning Guide. Mapleso, Waterloo Maple, Inc., Waterloo, Ontario, Canada.
57. Kattan, P.I. (2007). MATLAB Guide to Finite Elements, An Interactive Approach, 2nd Ed., Springer, Berlin, Germany.
58. Comsol 5.2 (2015). User's Manual, Comsol, Inc., Burlington, MA. Desai, C.S. (1979). Elementary Finite Element Method, Prentice-Hall, Inc., Englewood Clis, NJ.
59. Darrell W. Pepper and Juan C. Heinrich, The Finite Element Method: Basic Concepts and Applications, Third Edition, Published by CRC Press, New York.
60. Introduction To Comsol Multiphysics (Manual 2017 Version 5.3).
61. Nisheka Anadkat, M J S Rangachar, Simulation based Analysis of Capacitive Pressure Sensor with Comsol Multiphysics, International Journal of Engineering Research & Technology (IJERT) ISSN: 2278-0181 IJERTV4IS041064 [www.ijert.org](http://www.ijert.org) Vol. 4 Issue 04, April-2015
62. Rashed Al Amin and al., Simulation Analysis of Capacitive Pressure Sensor for MEMS Using Graphene, International Conference on Materials, Electronics & Information Engineering, ICMEIE-2015.
63. Veikko Lindroos and al. Handbook of Silicon Based MEMS Materials and Technologies, Applied Science Publishers, 2010.
64. <https://en.wikipedia.org/wiki/Tungsten>